OsOSCA2.4 regulates post-Golgi trafficking of storage proteins by modulating Ca^{2+} homeostasis in rice endosperm[1]

Yu Zhang[1, a], Yun Zhu[2, a], Pengcheng Zhang[1, a], Wang Tian[3], Hui Dong[1], Zebin Liu[4], Yu Chen[2], Xiuhao Bao[1], Tian Pan[1], Yehui Xiong[2], Xin Wang[2], Zhijie Ren[3], Xiaokang Jiang[1], Xiaohang Han[2], Ruonan Jing[1], Hongming Wu[1], Chuanwei Gu[1], Rongbo Chen[1], Xiaoli Chen[1], Jie Lei[1], Erchao Duan[1], Cailin Lei[2], Zhijun Cheng[2], Jiachang Wang[2], Yiqun Bao[5], Chuanyin Wu[2], Haiyang Wang[2], Yihua Wang[1]*, Yulong Ren[2]*, and Jianmin Wan[1,2]*

[1] State Key Laboratory for Crop Genetics & Germplasm Enhancement and Utilization, Zhongshan Biological Breeding Laboratory, Jiangsu Nanjing Rice Germplasm Resources National Field Observation and Research Station, Nanjing Agricultural University, Nanjing 210095, China.

[2] State Key Laboratory of Crop Gene Resources and Breeding, National Key Facility for Crop Gene Resources and Genetic Improvement, Institute of Crop Sciences, Chinese Academy of Agricultural Sciences, Beijing 100081, China.

[3] State Key Laboratory of Protein and Plant Gene Research, School of Advanced Agricultural Sciences, Peking University, Beijing 100871, China.

[4] College of Life Science, Capital Normal University, Beijing 100048, China.

[5] College of Life Sciences, Nanjing Agricultural University, Nanjing 210095, China.

[a] These authors contributed equally: Yu Zhang, Yun Zhu and Pengcheng Zhang

The author responsible for distribution of materials integral to the findings presented in this article in accordance with the policy described in the Instructions for Authors (https://academic.oup.com/plcell/pages/General-Instructions) is: Jianmin Wan (wanjm@njau.edu.cn).

© The Author(s) 2026. Published by Oxford University Press on behalf of American Society of Plant Biologists. All rights reserved. For commercial re-use, please contact reprints@oup.com for reprints and translation rights for reprints. All other permissions can be obtained through our RightsLink service via the Permissions link on the article page on our site—for further information please contact journals.permissions@oup.com.

ACCEPTED MANUSCRIPT

Downloaded from https://academic.oup.com/plcell/advance-article/doi/10.1093/plcell/koag193/8719692 by National Science & Technology Library user on 03 July 2026

*Author for correspondence: wanjm@njau.edu.cn, renyulong@caas.cn and yihuawang@njau.edu.cn

Short title: OsOSCA2.4 regulates storage proteins sorting

Abstract

Seed storage proteins (SSPs), which accumulate specifically during seed development, constitute a major source of plant-derived protein in the human diet. Despite their critical role in determining crop quality, the molecular mechanisms underlying the intracellular trafficking of SSPs remain poorly understood. Here, we characterize the rice *glutelin precursor accumulation16* (*gpa16*) mutant, which exhibits defective dense vesicle (DV)-mediated post-Golgi trafficking of proglutelins, resulting in their overaccumulation in the apoplast. *GPA16* encodes OsOSCA2.4, a member of the reduced hyperosmolality-induced Ca^{2+} increase channel (OSCA) family. OsOSCA2.4 localizes to post-Golgi compartments including the *trans*-Golgi network (TGN) and prevacuolar compartment (PVC) in vegetative tissue, and DVs in the endosperm. The OsOSCA2.4(P397L) variant disrupts the formation of the Rab5a molecular module, a process influenced by intracellular Ca^{2+} homeostasis. Ca^{2+} imaging assays indicate that OsOSCA2.4 functions as a regulator of Ca^{2+} homeostasis of PVCs/DVs, the primary sites of Rab5a module activity. Genetic analyses reveal functional redundancy between *OsOSCA2.4* and *OsOSCA4.1* in modulating post-Golgi trafficking of proglutelins. Collectively, our findings identify OSCA-mediated Ca^{2+} homeostasis as a previously unrecognized regulatory layer governing post-Golgi trafficking of SSPs and uncover an unexpected role for OSCA proteins in vesicular trafficking in eukaryotes.

Key words: Seed storage proteins, Post-Golgi trafficking, Ca^{2+} homeostasis

ACCEPTED MANUSCRIPT

Downloaded from https://academic.oup.com/plcell/advance-article/doi/10.1093/plcell/koag193/8719692 by National Science & Technology Library user on 03 July 2026

Introduction

In higher plants, seed storage proteins (SSPs) that accumulate specifically in seeds serve as a crucial source of nutrients for seed germination and seedling growth (Kawakatsu et al. 2010). More importantly, SSPs provide dietary proteins for humans and livestock, and their content and composition in seeds largely determine diverse quality traits for end uses in crops (Kawakatsu et al. 2010; Takaiwa et al. 2017). In addition, crop grains have also been successfully used as bioreactors for the production of recombinant proteins with pharmaceutical value, such as the rice seed-derived recombinant human serum albumin (Niu et al. 2025). Therefore, uncovering the molecular mechanisms underlying the intracellular synthesis, transport, and deposition of SSPs in plants is crucial for the genetic improvement of crop quality and genetic engineering.

SSPs are traditionally classified into albumins, globulins, prolamins, and glutelins based on their solubility (Osborne, 1924). Upon being initially synthesized in the endoplasmic reticulum (ER), SSPs are either directly deposited into ER-derived protein bodies (PBs), such as maize (*Zea mays*) zeins and rice (*Oryza sativa* L.) prolamins, or delivered to specialized vacuoles called protein storage vacuoles (PSVs) in a vesicle-mediated manner, such as soybean (*Glycine max*) SSPs and rice glutelins (Zheng et al. 2022a; Ren et al. 2022). Ultrastructural studies by transmission electron microscopy have revealed at least two distinct PSV transport pathways for SSPs: one is Golgi-independent pathway involving plant specific precursor-accumulating vesicles (PACs) (Takahashi et al. 2005) or autophagosomes (Ding et al. 2022), the other is Golgi-dependent pathway involving dense vesicles (DVs), known as a plant-unique vesicular carrier for post-Golgi trafficking of SSPs in most plant seeds (Otegui et al. 2006; Reyes et al. 2011). However, the molecular machineries required for plant-unique vesicle-mediated PSV transport pathways remain largely unknown in plant seeds.

Compared to most plant seeds that are dominated by a single SSP class (Heath et al. 1986; Shewry et al. 1995), rice seeds accumulate two major types of proteins: prolamins and glutelins, and store them in protein body I (PBI) and protein body II (PBII), respectively

ACCEPTED MANUSCRIPT

Downloaded from https://academic.oup.com/plcell/advance-article/doi/10.1093/plcell/koag193/8719692 by National Science & Technology Library user on 03 July 2026

(Kawakatsu et al. 2010). Together with its relatively small genome, these unique features have made rice a model system for dissecting the molecular mechanisms of intracellular transport of SSPs in crops (Ren et al. 2022). Glutelins, accounting for 60%-80% of total SSPs in rice seeds, are initially synthesized as precursors (also called proglutelins) in the ER, and then delivered to PSVs via the Golgi-dependent pathway (He et al. 2021; Ren et al. 2022; Zheng et al. 2022a), where they are processed into mature glutelin acidic and basic subunits by vacuolar processing enzyme OsVPE1 (Wang et al. 2009; Kumamaru et al. 2010). Genetic screening of *glutelin precursor accumulation* (*gpa*) and *glutelin precursor* (*glup*) mutants that abnormally accumulate proglutelins have identified and characterized several factors required for efficient proglutelin transport (Ueda et al. 2010; Fukuda et al. 2011; Wen et al. 2015; He et al. 2021; Zheng et al. 2022a; Ren et al. 2022). Among them, a critical molecular module for post-Golgi trafficking of proglutelins encompasses the small GTPase Rab5a and its guanine nucleotide exchange factor (GEF) VPS9a, mutations in these components cause mistargeting of proglutelins into apoplast instead of PSVs (Goh et al. 2007; Wang et al. 2010; Fukuda et al. 2011; Liu et al. 2013; Wen et al. 2015). Furthermore, two Rab5a effectors have also been revealed to be involved in mediating membrane fusion between compartments/vesicles and PSVs. One is the MON1-CCZ1 complex that is required for the indirect post-Golgi fusion between DV and PSV via pre-vacuolar compartment (PVC) (Pan et al. 2021); the other is GPA5 that mediates the direct fusion of DV with PSV through recruiting downstream tethering and fusion machinery (Ren et al. 2020). Interestingly, a plant-unique protein GPA3 has been demonstrated to interact with VPS9a to regulate DV-mediated PSV transport pathways (Ren et al. 2014). Despite these significant advances, our understanding of vesicular trafficking in post-Golgi trafficking of SSPs in plant seeds remains fragmented.

In addition to above molecular machinery required for vesicle transport itself, ionic homeostasis within compartments/vesicles has emerged as an important modulator of vesicle dynamic (Hay, 2007; Südhof, 2013; Reguera et al. 2015; Ashnest et al. 2015; Zhu et al. 2019; Zhu et al. 2021; Ruan et al. 2023). For instance, pH regulation in the *trans*-Golgi network (TGN) and PVC by NHX-type $Na^+(K^+)/H^+$ exchangers and vacuolar H^+-ATPases play essential roles in vesicle budding and targeting in plants (Reguera et al. 2015; Ashnest et al.

ACCEPTED MANUSCRIPT

Downloaded from https://academic.oup.com/plcell/advance-article/doi/10.1093/plcell/koag193/8719692 by National Science & Technology Library user on 03 July 2026

2015; Zhu et al. 2019; Zhu et al. 2021). In animals and yeast cells, the role of Ca^{2+} homeostasis within cellular compartments during vesicular trafficking has been well documented (Antebi and Fink, 1992; Deng et al. 2018). For example, Ca^{2+} homeostasis in the Golgi lumen, regulated by Ca^{2+} pumps such as secretory pathway Ca^{2+}/Mn^{2+} ATPase 1 (SPCA1) (Deng et al. 2018) in animal cells and PM-related Ca^{2+}-ATPase 1 (Pmr1) (Antebi and Fink, 1992) in yeast, respectively, are associated with the sorting and export of secretory proteins. However, the role and underlying molecular mechanisms of Ca^{2+} homeostasis in regulating vesicular trafficking of SSPs in plant cells remains largely unknown.

In this study, we characterized a new *gpa* mutant *gpa16*, which is defective in post-Golgi trafficking of proglutelins from DVs to PSVs, as evidenced by the abnormal deposition of proglutelins into apoplast. The causal gene underlying the mistargeting of proglutelins in *gpa16* is *OsOSCA2.4*, a member of reduced hyperosmolality-induced Ca^{2+} increase channel (OSCA, also known as Ca^{2+}-permeable stress-gated cation channels, CSCs). OsOSCA2.4 localizes to both TGN and PVC in vegetative tissues and DVs in developing endosperm. The Ososca2.4 variant impairs the interaction and membrane recruitment of the VPS9a-Rab5a molecular module. In addition, the Ososca2.4 variant with a P397L substitution specifically impairs Ca^{2+} homeostasis of PVCs. Interestingly, mimic mutation in OsOSCA4.1 (P450L), another PVC-localized OSCA member, caused the same trafficking defect as *gpa16*. Genetically, *OsOSCA2.4* functions redundantly with *OsOSCA4.1* to modulate glutelin trafficking in rice endosperm. Together, our results reveal a previously uncharacterized role of OSCA proteins in plant vesicular trafficking, and support a functional connection between Ca^{2+} homeostasis and vesicle-mediated post-Golgi trafficking of SSPs in plants.

Results

The *gpa16* mutant overaccumulates proglutelins in mature seeds

To gain insights into the regulatory mechanisms underlying SSPs transport from the ER to PSVs, we screened an ethyl methanesulfonate (EMS)-mutagenized pool of the *japonica* variety Kitaake, and identified a new *gpa* mutant, designated *gpa16*. The *gpa16* plants

ACCEPTED MANUSCRIPT

Downloaded from https://academic.oup.com/plcell/advance-article/doi/10.1093/plcell/koag193/8719692 by National Science & Technology Library user on 03 July 2026

showed no significant differences in plant height or tiller number throughout their life cycle compared to the wild-type (WT) Kitaake plants (Fig S1a-c). Notably, *gpa16* exhibited reduced grain thickness at maturity, resulting in a significantly lower 1000-grain weight than the WT (Fig S1d-g).

To explore the possible effect of *gpa16* mutation on SSP accumulation in seeds, we compared total SSP profiles between WT and *gpa16* dry seeds. In the WT, glutelins predominantly accumulated as mature acidic and basic subunits, whereas *gpa1*6 over-accumulated proglutelins, accompanied by reduced levels of mature subunits (Fig 1a). Immunoblot analyses using an antibody against the glutelin basic subunit further confirmed a significant defect in proglutelin processing in *gpa16* (Fig 1b,c). Binding protein 1 (BiP1) and protein disulfide isomerase like 1-1 (PDIL1-1) are well-characterized molecular chaperones required for proglutelins folding in the ER (Takemoto et al. 2002). The mutants defective in proglutelin folding or ER exit typically exhibit overaccumulation of both chaperones due to activation of unfolded protein response (Wang et al. 2016; Bao et al. 2023). Immunoblot analyses revealed no detectable differences in the abundance of BiP1 or PDIL1-1 between WT and *gpa16* seeds (Fig 1b), indicating that ER folding or export of proglutelins is not impaired in *gpa16*. Collectively, these results suggest that the *gpa16* mutation most likely disrupts post-Golgi trafficking of proglutelins in rice endosperm.

Impairment of DV-mediated post-Golgi trafficking of proglutelins in the *gpa16* mutant

To further investigate the subcellular defects of proglutelins sorting in the *gpa16* mutant, we examined developing endosperm from both WT and *gpa16* plants using semithin sections followed by Coomassie Brilliant Blue (CBB) staining. In WT endosperm, two types of PBs were readily discernible: round-shape PBIs, composed of prolamins, and irregular-shape PBIIs, which harbors glutelins (Fig 1d). Although the size and morphology of PBIs were comparable between WT and *gpa16*, PBIIs were significantly smaller in *gpa16* than those in the WT (Fig 1e). In addition, CBB-stained paramural bodies (PMBs) were readily observed in *gpa16* (Fig 1d). Furthermore, double immunofluorescence labeling with anti-glutelin and

ACCEPTED MANUSCRIPT

Downloaded from https://academic.oup.com/plcell/advance-article/doi/10.1093/plcell/koag193/8719692 by National Science & Technology Library user on 03 July 2026

anti-prolamin antibodies confirmed the mis-localization of glutelins to PMBs in *gpa16* (Fig 1f). Together, these observations indicate that the *gpa16* mutation impairs the intracellular transport of glutelins, at least in part, resulting in mistargeting of glutelins to PMBs rather than to PSVs.

To verify this defect at the ultrastructural level, we performed transmission electron microscopy (TEM) on ultrathin sections from developing endosperm of WT and *gpa16*. A typical cytological feature of *gpa*/*glup* mutants defective in ER exit of proglutelins is the disorganization of round PBIs, accompanied by the formation of abnormal ER-derived PBs containing both glutelins and prolamins (Wang et al. 2016; Bao et al. 2023). However, such a feature was not observed in *gpa16*, and ER morphology and PBI size in *gpa16* were largely indistinguishable from those of WT (Fig S2a-d), suggesting that the ER-to-Golgi transport is not compromised in *gpa16*. In contrast, poorly filled PBIIs and PMB structures are readily observed in *gpa16* (Fig S2e-h), consistent with the mis-deposition of glutelins observed by light microscopy (Fig 1d-f).

To pinpoint the precise location where proglutelins trafficking was disrupted, we performed immunogold labeling with endosperm samples prepared by high-pressure freezing/freeze-substitution (HPF/FS). In developing WT endosperm cells, DVs act as the major post-Golgi vesicular carriers for proglutelins delivery to PSVs (Ren et al. 2022). Typical single membrane-enclosed DVs were observed near the Golgi in both WT and *gpa16* (Fig 1g,h), indicating that the formation and budding of DVs from the Golgi and TGN are not affected in *gpa16*. Consistently, PSVs in *gpa16* displayed insufficient glutelins filling (Fig 1i,j). Notably, we found numbers of DVs near cell wall and observed possible fusions of DVs with plasma membrane (PM) in *gpa16* (Fig 1k,l). Continuous unloading of glutelins into the apoplast space likely contributed to the formation of PMB structures (Fig 1l,o). Collectively, these ultrastructural observations suggest that the *gpa16* mutation disrupts the transport of DVs to PSVs, leading to extracellular deposition of proglutelins in rice seeds.

GPA16 encodes the rice OSCA family protein OsOSCA2.4

ACCEPTED MANUSCRIPT

Downloaded from https://academic.oup.com/plcell/advance-article/doi/10.1093/plcell/koag193/8719692 by National Science & Technology Library user on 03 July 2026

To identify the gene responsible for *gpa16* phenotypes, we generated an F_2 segregating population by crossing *gpa16* with the *indica* variety Dular. A total of 335 F_2 individuals exhibiting the typical mutant phenotype were used for map-based cloning. The *gpa16* locus was ultimately delimited to a 185-kb physical interval on chromosome 12 containing 16 annotated genes (Fig 2a). Genomic sequencing analysis revealed a single C-to-T nucleotide substitution in the 7th exon of *Os12g0582800* in *gpa16*, resulting in a proline (P) to leucine (L) substitution at the amino acid position 397 (P397L) (Fig 2b).

To determine whether the P397L substitution is responsible for *gpa16* phenotypes, we conducted a complementation experiment by introducing the full-length genomic fragment of *Os12g0582800*, including a 2113-bp upstream promoter region and an 891-bp downstream regulatory sequence, into homozygous *gpa16* calli. All positive transgenic lines fully restored wild-type phonotypes. Specifically, proglutelin accumulation was substantially reduced in the positive transgenic lines relative to the *gpa16* mutant, while the levels of mature acidic and basic glutelin subunits were correspondingly elevated (Fig 2c). Moreover, PBII morphology in positive transgenic lines were restored to WT phonotypes, and the PMB structures, specifically present in *gpa16*, is absent in these lines as well (Fig 2d). Unexpectedly, knockout of *GPA16* in the WT background did not cause the proglutelins accumulation phenotype observed in *gpa16* (Fig S3a,b). Interestingly, transgenic lines overexpressing *Os12g0582800* with the P397L substitution in the WT background phenocopied the *gpa16* mutant, exhibiting increased accumulation of proglutelins and reduced levels of mature acidic and basic glutelin subunits. In contrast, overexpression of *Os12g0582800* from the WT background had no detectable effect on the SSP accumulation (Fig S3c), indicating a possible dosage-dependent gain-of-function effect of the *gpa16* mutation. Collectively, these findings demonstrate that *Os12g0582800* corresponds to *GPA16*, and that the P397L substitution is sufficient to disrupt post-Golgi trafficking of proglutelins in rice endosperm.

BLAST analysis indicated that *GPA16* is a single-copy gene in the rice genome. Reverse transcription quantitative PCR (RT-qPCR) analysis revealed that *GPA16* is ubiquitously expressed in all tissues tested, with relatively higher transcript levels in the leaf sheath and

ACCEPTED MANUSCRIPT

Downloaded from https://academic.oup.com/plcell/advance-article/doi/10.1093/plcell/koag193/8719692 by National Science & Technology Library user on 03 July 2026

developing endosperm (Fig 2e,f). Notably, *GPA16* expression progressively increased during endosperm development, consistent with its role in SSP transport (Fig 2f). The GPA16 protein was annotated as OsOSCA2.4, a member of rice OSCA family (Fig 2g) (Yuan et al. 2014; Hou et al. 2014; Thor et al. 2020; Pei et al. 2024). For clarity, we hereafter refer to GPA16 as OsOSCA2.4, and mutated protein in *gpa16* as Ososca2.4. Hydrophobicity analyses predicted that OsOSCA2.4 contains 11 transmembrane α-helices, indicating that a large portion of the protein is embedded within the lipid bilayer (Fig 2h). AlphaFold-based structural prediction further revealed that the P397L substitution in Ososca2.4 is located in the fourth transmembrane α-helix (Fig 2h).

OsOSCA2.4 localizes to post-Golgi compartments, and self-interacts on the PVC

To investigate the *in vivo* function of OsOSCA2.4, we generated transgenic lines overexpressing *OsOSCA2.4* fused with either the green fluorescent protein (*GFP*) or a *Flag* tag driven by the 35S promoter in the *gpa16* background. Transgenic grains expressing either *OsOSCA2.4-GFP* or *OsOSCA2.4-Flag* restored wild-type phenotypes, including substantially reduced proglutelins accumulation and correspondingly elevated levels of mature acidic and basic subunits compared to the *gpa16* mutant (Fig S4), indicating that both fusion proteins are biologically functional *in vivo*.

We next used complemented *OsOSCA2.4-GFP* plants to visualize subcellular localization of OsOSCA2.4 *in vivo*. Confocal imaging revealed a punctate localization pattern of OsOSCA2.4-GFP in the coleoptile cells (Fig S5a). Given this punctate pattern and the possible roles of OsOSCA2.4 in post-Golgi trafficking of proglutelins, we coexpressed OsOSCA2.4-GFP with organelle markers characteristic for the Golgi (GmMan1-mRFP), TGN (mRFP-AtSYP61), and PVC (mRFP-AtVSR2), respectively, in leaf epidermal cells of *Nicotiana benthamiana* (Nebenführ et al. 1999; Sanderfoot et al. 2001; Miao et al. 2006). Confocal microscopy revealed that OsOSCA2.4-GFP partially co-localized with both TGN and PVC markers, as quantified by Pearson's correlation coefficients (PCCs) (Fig 3a).

ACCEPTED MANUSCRIPT

Downloaded from https://academic.oup.com/plcell/advance-article/doi/10.1093/plcell/koag193/8719692 by National Science & Technology Library user on 03 July 2026

To further validate the localization of OsOSCA2.4 in developing endosperm, we performed immunogold labeling on high-pressure frozen/freeze-substituted sections from *OsOSCA2.4-GFP* complemented lines using an anti-GFP antibody. Gold particles were specifically enriched on DVs (Fig S5b), consistent with a role for OsOSCA2.4 in post-Golgi trafficking of proglutleins in endosperm cells. To determine whether the P397L mutation affects the subcellular localization of OsOSCA2.4, we performed live-cell imaging analyses and found that the localization pattern of Ososca2.4 was largely indistinguishable from that of wild-type OsOSCA2.4 in both transgenic rice and *N. benthamiana* (Fig S5a,c). Collectively, these results demonstrate that OsOSCA2.4 localizes to post-Golgi compartments including the TGN and PVC, contrasting markedly with the previously reported PM-localized OSCA channels (Yuan et al. 2014; Thor et al. 2020; Pei et al. 2024).

Previous studies have shown that OSCA proteins usually function as homodimers (Jojoa-Cruz et al. 2018; Murthy et al. 2018; Zhang et al. 2018; Liu et al. 2018; Maity et al. 2019; Zhang et al. 2023; Jojoa-Cruz et al. 2024; Han et al. 2024). Consistent with this, yeast two-hybrid (Y2H) assays revealed strong self-interaction of both wild-type OsOSCA2.4 and the P397L variant Ososca2.4, as well as heterotypic interaction between the wild-type and mutant proteins (Fig 3b). This self-interaction was further confirmed using *in vivo* firefly luciferase complementation imaging (LCI) and co-immunoprecipitation (Co-IP) assays in *N. benthamiana* (Fig 3c,d). Moreover, bimolecular fluorescence complementation (BiFC) assays revealed strong fluorescence signals specifically on the PVC, indicating that OsOSCA2.4 self-dimerization occurs at this compartment (Fig 3e). Collectively, these results suggest that OsOSCA2.4 might function as a homodimer or oligomer on the PVC.

The *Ososca2.4* mutation impairs the membrane association of Rab5a and VPS9a

In rice seed, Rab5a and its GEF VPS9a can form a molecular module that controls DV-mediated post-Golgi trafficking of SSPs (Wang et al. 2010; Liu et al. 2013; Ren et al. 2014; Ren et al. 2020). Given that OsOSCA2.4 localized to DV in developing endosperm (Fig S5b), we asked whether OsOSCA2.4 is functionally linked to the Rab5a molecular module in rice

ACCEPTED MANUSCRIPT

Downloaded from https://academic.oup.com/plcell/advance-article/doi/10.1093/plcell/koag193/8719692 by National Science & Technology Library user on 03 July 2026

endosperm. We first tested whether OsOSCA2.4 physically interacts with either Rab5a or VPS9a. However, neither Y2H nor LCI assays detected a direct interaction between OsOSCA2.4 or its P397L variant (Ososca2.4) and components of the Rab5a molecular module (Fig S6).

We next examined whether the Ososca2.4 variant affects the interaction between the Rab5a and VPS9a. LCI assay showed that when coexpressed with *OsOSCA2.4*, the VPS9a-Rab5a interaction was comparable to that observed in control (Fig 4a). In contrast, coexpression with *Ososca2.4* substantially weakened this interaction, as manifested by reduced fluorescence signals (Fig 4a). Furthermore, BiFC assay with mCherry as an internal expression control revealed a substantial decrease in yellow fluorescence protein (YFP) fluorescence intensity upon coexpression with *Ososca2.4*, compared to WT or empty vector control (Fig S7a,b). As a negative control, *Ososca2.4* overexpression did not substantially influence the interaction of Golgi Transport 1B (GOT1B) and Sec23c in ER exit sites (ERESs), where these two proteins function cooperatively in the COPII-mediated ER exit of proglutelins in rice (Wang et al. 2016; Ren et al. 2022) (Fig S7c,d). Consistently, Co-IP assay also verified the detrimental effect of Ososca2.4 on the Rab5a-VPS9a interaction (Fig 4b). Together, these results indicate that Ososca2.4 variant interferes with the formation of the Rab5a molecular module in plants.

We next examined whether *Ososca2.4* expression affects the subcellular distribution of the Rab5a molecular module by transforming functional GFP-tagged Rab5a and VPS9a into the WT and *gpa16* backgrounds (Ren et al. 2020). In WT, both fusion proteins constantly localized to the cytosol and punctate compartments (Fig 4c), consistent with previous reports (Wang et al. 2010; Ren et al. 2020). By contrast, in the *gpa16* background, the punctate localization of Rab5a and VPS9a was dramatically diminished, as confirmed by quantitative analysis (Fig 4c,d). As a control, the subcellular localization pattern of vesicle-associated membrane protein 727 (VAMP727), a SNARE component required for post-Golgi trafficking of SSPs in plants (Takemoto et al. 2018), was indistinguishable between WT and *gpa16* cells (Fig 4c,d).

ACCEPTED MANUSCRIPT

Downloaded from https://academic.oup.com/plcell/advance-article/doi/10.1093/plcell/koag193/8719692 by National Science & Technology Library user on 03 July 2026

Consistent with above confocal imaging data, subcellular fractionation of developing endosperm followed by immunoblotting revealed a dramatically reduced proportion of Rab5a and VPS9a in the membrane fraction of *gpa16* compared with the WT (Fig 4e,f). As controls, UDP-glucose pyrophosphorylase (UGPase) (Kleczkowski et al. 2010) and tonoplast intrinsic protein 3-1 (TIP3-1) (Takahashi et al. 2004) were detected exclusively in the cytosolic (S100) and the membrane fractions (P100), respectively (Fig 4e). These confocal imaging and biochemical data demonstrate that the Ososca2.4 variant disrupts the membrane recruitment of Rab5a and VPS9a in developing endosperm. To determine whether Rab5a or VPS9a influences the subcellular localization of OsOSCA2.4, we expressed *OsOSCA2.4-GFP* in the *rab5a* and *vps9a* mutant backgrounds. Depletion of either protein did not substantially alter the punctate localization pattern of OsOSCA2.4-GFP (Fig S8). Taken together, these results indicate that *OsOSCA2.4* likely functions upstream of *Rab5a* and *VPS9a* in the post-Golgi trafficking of glutelins in rice endosperm.

Ca^{2+} transients in the cytosol is required for the membrane association of the Rab5a molecular module

Ca^{2+} has been shown to regulate vesicular trafficking mediated by small Rab GTPase in eukaryotic cells (Parkinson et al. 2014; Langemeyer et al. 2018). Given that OsOSCA2.4 may be a putative Ca^{2+}-related regulator onto intracellular vesicles, supported by its structural homology to canonical OSCA family members and its subcellular localization to post-Golgi compartments/vesicles (Fig 2h; Fig 3a; Han et al, 2024), it is possible that defective Rab5a module recruitment to vesicular membranes arises from perturbed intracellular Ca^{2+} homeostasis. To test this hypothesis, we examined whether intracellular Ca^{2+} conditions are required for the interaction between Rab5a and VPS9a in plants.

We first manipulated cytosolic Ca^{2+} levels using Ca^{2+} ionophore ionomycin and the Ca^{2+} chelator ethylene glycol tetraacetic acid (EGTA), and monitored dynamic changes in cytosolic Ca^{2+} concentrations using the genetically encoded Ca^{2+} indicator GCaMP6s (Chen et al. 2013). Ionomycin and EGTA treatment induced a robust increase in GCaMP6s

ACCEPTED MANUSCRIPT

Downloaded from https://academic.oup.com/plcell/advance-article/doi/10.1093/plcell/koag193/8719692 by National Science & Technology Library user on 03 July 2026

fluorescence intensity, confirming elevated cytosolic Ca^{2+} levels in plant cells. In contrast, free GFP fluorescence remained unaffected by these treatments (Fig S9), verifying the specificity of the Ca^{2+}-dependent response. Notably, pharmacological elevation of cytosolic Ca^{2+} significantly enhanced the Rab5a-VPS9a interaction, as quantified by BiFC signal intensity (Fig 4g,h). To further substantiate the functional relationship between cytosolic Ca^{2+} dynamics and Rab5a module membrane association, we treated roots of transgenic plants expressing functional Rab5a-GFP or VPS9a-GFP with EGTA-AM, a cell-permeant Ca^{2+} chelator that depletes intracellular Ca^{2+} stores. As anticipated, EGTA-AM treatment led to a pronounced reduction in punctate GFP fluorescence signals for both Rab5a and VPS9a proteins (Fig 4i,j), indicating impaired membrane recruitment of the Rab5a module upon intracellular Ca^{2+} depletion. Collectively, these results indicate that physiological cytosolic Ca^{2+} conditions play crucial roles in maintaining the membrane association and functional integrity of the Rab5a module in plant cells.

The P397L mutation in OsOSCA2.4 specifically disrupts Ca^{2+} homeostasis of PVCs

To investigate Ca^{2+} dynamics in distinct post-Golgi compartments, we engineered a suite of compartment-targeted variants of the ratio-metric Ca^{2+} biosensor YC3.6 (yellow cameleon version 3.6) (Nagai et al. 2004). Specifically, YC3.6 was fused to well-characterized targeting sequences to direct its localization to TGN, PVC, or cytosol (designated YC3.6-TGN, YC3.6-PVC, and YC3.6-CYT, respectively; Fig 5a-c). These constructs were transiently expressed in rice protoplasts isolated from WT and *gpa16* plants to enable comparative quantification of compartmental or cytosolic Ca^{2+} levels. Confocal imaging revealed a dramatic and consistent reduction in luminal Ca^{2+} concentration within PVCs of *gpa16* protoplasts compared with the WT controls (Fig 5d,e). In contrast, no statistically robust difference in TGN luminal Ca^{2+} levels was detected in *gpa16* relative to the WT (Fig 5d,e). Also, cytosolic Ca^{2+} levels, as reported by YC3.6-CYT, remained indistinguishable between WT and *gpa16* (Fig 5d,e). Importantly, complementation with the functional OsOSCA2.4-Flag fusion protein fully restored PVC luminal Ca^{2+} levels in *gpa16* (Fig 5f,g). Taken together, these results

ACCEPTED MANUSCRIPT

Downloaded from https://academic.oup.com/plcell/advance-article/doi/10.1093/plcell/koag193/8719692 by National Science & Technology Library user on 03 July 2026

suggest that the P397L substitution in OsOSCA2.4 selectively impairs Ca^{2+} homeostasis specifically within PVCs, without broadly disrupting cytosolic or TGN luminal Ca^{2+} pools.

To further investigate whether OsOSCA2.4 specifically modulates the Ca^{2+} microenvironment at the outer surface of PVC, we constructed a Ca^{2+} sensor targeted to the PVC surface by fusing the Ca^{2+} biosensor GCaMP6s with the PI3P-binding domain 2×FYVE (Gao et al, 2014). An mCherry fluorescent reporter was co-expressed via a self-cleaving 2A peptide linker to serve as an internal control for expression level (Fig 5h) (Szymczak et al, 2004). The construct mCherry-2A-GCaMP6s-2×FYVE was transiently expressed in protoplasts isolated from WT and the *gpa16* mutant plants (Fig 5i,j). Relative Ca^{2+} levels at the PVC surface were quantified as the ratio of GCaMP6s-derived GFP fluorescence intensity to mCherry fluorescence intensity. As anticipated, the GFP/mCherry ratio was significantly reduced in *gpa16* relative to the WT (Fig 5i,j), indicating that Ca^{2+} activity at the PVC surface is impaired in the *gpa16* mutant (Fig 5i,j). Collectively, these results suggest that OsOSCA2.4 may function as a putative regulator of Ca^{2+} homeostasis on the PVC.

To investigate whether OsOSCA2.4 and its P397L variant differentially modulate Ca^{2+} homeostasis in response to mechanical stimuli, as previously reported *Arabidopsis* OSCA proteins (Murthy et al. 2018; Zhang et al. 2018; Maity et al. 2019; Zhang et al. 2023; Jojoa-Cruz et al. 2024; Han et al. 2024), we tried to generate PM-targeted variants of both proteins. We first validated the membrane topology of OsOSCA2.4 using a proteinase K protection assay, which confirmed cytosolic exposure of its C-terminus (Fig S10a). Subsequently, we introduced two point mutations to abolish endosomal sorting of both proteins: substitution of the two LL-based sorting motifs in the cytosolic loop to LV (mimicking AtOSCA1.1/1.2; Schmidt et al. 2006), and replacement of the C-terminal LL motif with AA (Fig S10b-d; Fig 5k). These constructs (OsOSCA2.4-LV-AA and Ososca2.4-LV-AA) were separately coexpressed in *N. benthamiana* leaves together with the cytosolic Ca^{2+} biosensor GCaMP6s (Fig 5l). Mechanical perturbation was induced by treatment with 1 mM β-cyclodextrin (βCD), known as a pharmacological inducer of PM tension (Cox et al. 2021). Quantitative analyses of GCaMP6s fluorescence dynamics showed that βCD-induced Ca^{2+} transients were significantly diminished in leaves expressing Ososca2.4-LV-AA compared to those

ACCEPTED MANUSCRIPT

Downloaded from https://academic.oup.com/plcell/advance-article/doi/10.1093/plcell/koag193/8719692 by National Science & Technology Library user on 03 July 2026

expressing OsOSCA2.4-LV-AA (Fig 5l,m), demonstrating that the P397L substitution specifically compromises the mechanotransduction function of OsOSCA2.4 in plant cells.

To directly assess the intrinsic channel activity of OsOSCA2.4, we heterologously expressed C-terminally GFP-tagged OsOSCA2.4 and Ososca2.4 in HEK293T cells and *Xenopus laevis* oocytes. Both constructs exhibited clear PM localization in oocytes, while they were targeted to the cytosol in HEK293T cells (Fig S11a,b). Unfortunately, we failed to detect osmotic stress- or voltage-induced currents in oocytes expressing OsOSCA2.4 or Ososca2.4, although extensive efforts were made (Fig S11c,d). In contrast, oocytes expressing AtCNGC2 or AtCNGC4 displayed voltage-induced currents as reported in previous study (Fig S11d; Tian et al. 2019).

OsOSCA2.4 functions redundantly with _OsOSCA4.1_ to regulate post-Golgi trafficking of proglutelins in rice

Since knockout of *OsOSCA2.4* did not result in detectable defects in proglutelin trafficking in endosperm (Fig S3a,b), we hypothesized that OsOSCA2.4 may function redundantly with other OSCA homologs. The rice genome encodes 11 putative OSCA proteins, which are categorized into 4 subfamilies (Fig 2g). We therefore examined the subcellular localization of all 11 OSCA proteins in *N. benthamiana*, and found that OsOSCA4.1, similar to OsOSCA2.4, displays dual localization to both TGN and PVC (Fig 6a). Moreover, Y2H assay showed that OsOSCA4.1 is also capable of self-interaction (Fig 6b).

To test potential functional redundancy of these two genes, we produced a P450L substitution into OsOSCA4.1 to mimic the P397L substitution in OsOSCA2.4, and expressed this mutant variant in the WT background (Fig S12). Notably, overexpression of *OsOSCA4.1-P450L* resulted in phenotypes resembling those of the *gpa16* mutant (Fig 6c,d). Furthermore, we employed the CRISPR-Cas9 strategy to generate single and double mutants of *OsOSCA2.4* and *OsOSCA4.1* (Fig 6e). Immunoblot analyses coupled with quantitative measurements showed that, similar to the knockout mutant of *OsOSCA2.4* single mutant, the *OsOSCA4.1* single mutant was indistinguishable from the WT, whereas the *Ososca2.4-*

ACCEPTED MANUSCRIPT

Downloaded from https://academic.oup.com/plcell/advance-article/doi/10.1093/plcell/koag193/8719692 by National Science & Technology Library user on 03 July 2026

2 Ososca4.1 double mutant exhibited pronounced accumulation of proglutelins in dry seeds (Fig 6f,g). Collectively, this genetic evidence supports the notion that *OsOSCA2.4* functions redundantly with *OsOSCA4.1* to modulate post-Golgi trafficking of proglutelins in rice endosperm.

Discussion

SSPs provide a high-quality source for dietary protein for humans and livestock, and their abundance and composition largely determine multiple quality traits of crop grains (Kawakatsu et al. 2010; Takaiwa et al. 2017). Plants have evolved plant-unique vesicular carriers, such as PAC vesicle and DV, to guarantee highly efficient transport of SSPs in developing seeds (Takahashi et al. 2005; Otegui et al. 2006; Reyes et al. 2011). Despite extensive cytological characterization, the molecular mechanisms controlling DV-mediated post-Golgi trafficking of SSPs remain exclusive. In this study, through a forward genetic approach, we identified a gain-of-function variant of OsOSCA2.4 and demonstrated that Ososca2.4 mutation substantially influences post-Golgi trafficking of proglutelins in rice endosperm (Fig 1; Fig 2). At the biochemical level, Ososca2.4 attenuates the interaction between Rab5a and VPS9a, and dramatically impairs their membrane recruitment in developing endosperm cells (Fig 4). This interaction between Rab5a and VPS9a was also disrupted by perturbations in intracellular Ca^{2+} homeostasis (Fig 4). Notably, the Ososca2.4 specifically affects the Ca^{2+} homeostasis at the PVC, where Rab5a and VPS9a act to regulate the directional targeting of proglutelins (Fig 5). Consequently, Ososca2.4 interferes with the directional targeting of DVs to PSVs, likely by perturbing Ca^{2+} homeostasis of vesicles in rice endosperm (Fig 2; Fig 5). Notably, genetic analyses reveal that OsOSCA2.4 functions redundantly with another post-Golgi compartment-localized OSCA family member, OsOSCA4.1, to regulate DV-mediated post-Golgi trafficking of SSPs in rice endosperm (Fig 6). Altogether, our findings uncover OSCA-mediated Ca^{2+} homeostasis of vesicle as a critical mechanism in modulating post-Golgi trafficking of proglutelins in rice, thereby advancing our understanding of plant-unique vesicular trafficking pathways in plant seeds.

ACCEPTED MANUSCRIPT

Downloaded from https://academic.oup.com/plcell/advance-article/doi/10.1093/plcell/koag193/8719692 by National Science & Technology Library user on 03 July 2026

The importance of organellar Ca^{2+} homeostasis in vesicular trafficking has been well documented in animals and yeast cells, where Ca^{2+} pumps such as SPCA1 and Pmr1 play central roles in Golgi function, protein sorting, and vesicle export (Antebi and Fink, 1992; Hay, 2007; Lelouvier and Puertollano, 2011; Kilpatrick et al. 2013; D'hooge et al. 2015; Deng et al. 2018; Hu et al. 2024). However, comparable regulators of vesicle-associated Ca^{2+} homeostasis in plants remain largely unknown. Here, we identify OsOSCA2.4 as a regulator of Ca^{2+} homeostasis specifically in the PVC in plants (Fig 5). Similar to the Rab5a molecular machinery (Goh et al. 2007; Wang et al. 2010; Fukuda et al. 2011; Liu et al. 2013; Wen et al. 2015), OsOSCA2.4 localizes to PVC in vegetative tissues (Fig 3) and to DV in developing endosperm (Fig S5). Although live-cell Ca^{2+} imaging in developing endosperm cells remains technically challenging, our use of organelle-specific Ca^{2+} biosensors in rice protoplasts demonstrates that OsOSCA2.4 is required for maintaining Ca^{2+} homeostasis across PVCs (Fig 5). Unlike vesicle-localized SPCA1 and Pmr1, which function in regulating luminal Ca^{2+} homeostasis within the Golgi apparatus (Antebi and Fink, 1992; Deng et al. 2018), OsOSCA2.4 most likely affects Ca^{2+} microenvironment at the cytosolic surface of vesicles, evidenced by the disrupted interaction and membrane recruitment of the membrane-associated Rab5a module (Fig 4,5). This mode of regulation is reminiscent of recent findings showing that Ca^{2+} transients at the cytosolic surface of the ER are crucial for autophagosome initiation (Zheng et al. 2022b). Our previous studies reveal that the Rab5a-centred molecular cascade is required for targeting, tethering, and fusion of DV to and with PSVs (Wang et al. 2010; Liu et al. 2013; Ren et al. 2014; Ren et al. 2020; Pan et al. 2021; Ren et al. 2022). The present work further identifies Ca^{2+} homeostasis as an important factor to modulate DV-mediated post-Golgi trafficking of SSPs in rice seeds.

OSCA family proteins were initially identified in *Arabidopsis* as hyperosmolality-activated, non-selective cation channels permeable to Ca^{2+} (Yuan et al. 2014; Hou et al. 2014). Notably, OSCA proteins with definite channel activity in plants are generally localized to the PM (Yuan et al. 2014; Thor et al. 2020; Pei et al. 2024), in sharp contrast to the post-Golgi compartment localization of OsOSCA2.4 and OsOSCA4.1 characterized in this study (Fig 3; Fig 6). Although patch-clamp techniques have been successfully applied to characterize PM- and vacuole-

ACCEPTED MANUSCRIPT

Downloaded from https://academic.oup.com/plcell/advance-article/doi/10.1093/plcell/koag193/8719692 by National Science & Technology Library user on 03 July 2026

localized channels in plants (Hedrich, 2012), determining the channel activity of proteins in vesicle remains technically challenging. Although OsOSCA2.4 successfully localized to the PM when expressed in *X. laevis* oocytes, electrophysiological assays did not detect hyperosmolality- or voltage-induced currents for OsOSCA2.4, including its variant Ososca2.4 (Fig S11). A possible explanation is that the heterologous membrane embedding of OsOSCA2.4 in the PM of oocytes disrupts its channel activity. Given that vesicular trafficking involves substantial membrane curvature and dynamic membrane tension during budding and fusion, and that OSCA proteins are mechanosensitive channels activated by lipid-mediated forces, it is plausible that OsOSCA2.4 is mechanically activated within the highly curved membranes of DVs in rice endosperm (Bonifacino and Glick, 2004; Jojoa-Cruz et al. 2018; Murthy et al. 2018; Zhang et al. 2018; Maity et al. 2019; Guichard et al. 2022; Zhang et al. 2023; Jojoa-Cruz et al. 2024; Han et al. 2024). Alternatively, OsOSCA2.4 may be gated through mechanisms distinct from those described for AtOSCA1.1 and AtOSCA1.2 (Hou et al. 2014; Yuan et al. 2014). Indeed, diverse modes of Ca^{2+} channel activation have been reported, including protein-mediated activation (e.g. BIK1-activated AtOSCA1.3), small-molecule-activated channels, cyclic nucleotide-gated channels, and inositol trisphosphate-gated IP_3 receptors (Yau, 1994; Thor et al. 2020; Woll and Van Petegem, 2022). Another possibility is that OsOSCA2.4 may function as a Ca^{2+} sensor, potentially interacting with other partners to modulate Ca^{2+} transport of DVs, thereby maintaining the efficient recruitment and formation of the Rab5a module in rice endosperm. Future studies should aim to investigate whether and how OsOSCA2.4 and OsOSCA4.1 directly function as a Ca^{2+} channel in endosperm cells and to define the precise mechanisms by which vesicle-associated Ca^{2+} dynamics regulate post-Golgi trafficking of SSPs in plants.

ACCEPTED MANUSCRIPT

Downloaded from https://academic.oup.com/plcell/advance-article/doi/10.1093/plcell/koag193/8719692 by National Science & Technology Library user on 03 July 2026

Materials and Methods

Plant materials and growth conditions

The *gpa16* mutant described in this study was isolated from an ethyl methanesulfonate (EMS)-mutagenized pool of *japonica* cultivar Kitaake. To minimize background mutations, the *gpa16* mutant was backcrossed at least three times with the corresponding wild type (WT) Kitaake. Unless otherwise stated, all plant materials were cultivated either in paddy fields throughout typical growing seasons or in a controlled greenhouse environment at the Chinese Academy of Agricultural Sciences (Beijing, China).

Antibodies

Antibodies against the glutelin basic subunits, BiP1, PDIL1-1, VPS9a, and TIP3-1 were described previously (Wang et al. 2010; Wang et al. 2016; Ren et al. 2020). Commercially available antibodies used in this study included anti-GFP (1:5,000; Roche, 11814460001), anti-Flag (1:5,000; Sigma-Aldrich, F1804), anti-EF-1α (1:5,000; Agrisera, AS10934), and anti-UGPase (1:3,000; Agrisera, AS05086).

Protein extraction related assays

Total protein extraction from dry seeds was performed as previously described (Ren et al. 2014; Ren et al. 2020). Briefly, mature seeds were ground into flour, followed by the addition of lysis buffer containing 4% (w/v) SDS, 4 M urea, 5% (v/v) β-mercaptoethanol, and 125 mM Tris-HCl (pH 6.8) and incubation at room temperature overnight. Unless otherwise noted, 25 μL lysis buffer was added to 1 mg of rice flour.

For protein extraction from plants or developing endosperm, 10-day-old plant seedlings, developing endosperm or *N. benthamiana* leaves were ground to powder in liquid nitrogen. The samples were then resuspended in ice-cold NB1 buffer containing 50 mM Tris-MES (pH 8.0), 1 mM $MgCl_2$, 0.5 M Sucrose, 10 mM EDTA (pH 8.0), 5 mM DTT, 0.1% (v/v) Nonidet P-40, and 1×Complete Protease Inhibitor Cocktail. Homogenates were incubated at 4°C for 20 min, filtered through cheesecloth to remove cell debris, and centrifuged at 10,000*g* for 10 min at 4°C for subsequent analyses.

ACCEPTED MANUSCRIPT

Downloaded from https://academic.oup.com/plcell/advance-article/doi/10.1093/plcell/koag193/8719692 by National Science & Technology Library user on 03 July 2026

Subcellular fractionation was performed by grinding developing endosperm in liquid nitrogen, and resuspending the powder in ice-cold NB1 buffer without detergent. After centrifugation at 2,000*g* for 5 min to remove debris, the supernatant was ultracentrifuged at 100,000*g* for 90 min at 4°C to obtain the soluble fraction (S100) and membrane fraction (P100). Fractions were mixed 5× protein loading buffer, boiled at 100°C for 5 min, and subjected to immunoblot analysis.

To determine membrane topology of OsOSCA2.4, *OsOSCA2.4-GFP* driven by the 35S promoter was expressed in *N. benthamiana* for 48-72 h. Leaf samples were ground into flour in liquid nitrogen before adding ice-cold NB1 buffer (without Nonidet P-40). The filtered homogenate was centrifugated at 2,000*g* for 5 min to remove debris. The membrane fraction (P100) was obtained by ultracentrifugation at 100,000*g* for 90 min at 4°C. The P100 fraction was resuspended in NB1 buffer with or without 1% (v/v) Triton X-100, and incubation with 10 ng/μL proteinase K for 15 min on ice. The reactions were terminated by adding 5 mM phenylmethylsulfonyl fluoride (PMSF).

Unless otherwise specified, 1.5 mL NB1 buffer was added for 1 g of plant tissues and 1 mL for 1 g of developing endosperm samples.

Immunoblot analyses

For immunoblot analyses, protein samples were separated by SDS-PAGE using 12.5% (v/v) uniform gels and transferred to nitrocellulose membranes (Cytiva). Membranes were blocked in PBST (PBS containing 0.1% Tween 20 (v/v)) supplemented with 5% (w/v) skim milk. Subsequently, the membranes were incubated with appropriate primary antibodies. Antibody-antigen reactions were detected using an ECL detection reagent (Thermo Fisher Scientific), and the resulting signals were visualized using the ChemiDoc MP imaging system. Band intensities were quantified using the ImageJ program (https://imagej.nih.gov/ij/).

Map-based cloning

To map the *GPA16* locus, the *gpa16* mutant was crossed with the *indica* var. Dular and produced an F_2 segregating population. As described previously (Ren et al. 2020), individual

ACCEPTED MANUSCRIPT

Downloaded from https://academic.oup.com/plcell/advance-article/doi/10.1093/plcell/koag193/8719692 by National Science & Technology Library user on 03 July 2026

seeds with floury endosperm from the F_2 segregating population was used to map the *GPA16* gene. Molecular markers utilized for fine mapping are listed in Data S1.

Generation of transgenic plants

For complementation test, an 8,681-bp WT genomic fragment spanning the regulatory elements (nucleotides -2,113 bp to 6,565 bp from ATG) was cloned into the pCAMBIA2300 vector (CAMBIA) to generate the *pGPA16:GPA16* construct. For the GFP-tagged (or Flag-tagged) *GPA16/OsOSCA2.4* or *gpa16/Ososca2.4* transgenic plants, the coding sequence of *GPA16*/*OsOSCA2.4* or *gpa16*/*Ososca2.4* was amplified and inserted into the binary vector pCAMBIA1305GFP or pCAMBIA1300-221-Flag with a 35S promoter (Ren et al., 2020). For ubiquitin promoter-driven expression, the same coding sequences were cloned into pCAMBIA1305GFP downstream of the maize *UBIQUITIN* promoter.

To generate *Ososca2.4* and *Ososca4.1* knockout mutant mediated by the CRISPR-Cas9-based genome editing, sgRNA targeting each gene was designed using CRISPR-P (http://cbi.hzau.edu.cn/cgi-bin/CRISPR). Target fragments were ligated into Cas9-sgRNAvector. The resulting constructs were transformed into Kitaake, and transgenic lines were genotyped by PCR and sequencing.

Construction of vectors for *Rab5a-GFP* or *VPS9a-GFP* driven by their native promoters was described previously (Wang et al. 2010; Liu et al. 2013). Unless indicated otherwise, vectors were prepared using double restriction enzyme digestion (Thermo Fisher Scientific), and all constructs were generated using an infusion cloning kit (Clontech). The constructed binary vectors were individually introduced into *Agrobacterium tumefaciens* strain EHA105, and the resulting lines were used to infect rice calli of Kitaake, *gpa16/Ososca2.4*, *rab5a* or *vps9a*.

For site-specific mutagenesis of OsOSCA4.1, protein alignment of 11 OsOSCAs was generated by SnapGene 6.0.2. The proline residue at position 450 of OsOSCA4.1, corresponding to P397 of OsOSCA2.4, was substituted with leucine by replacing the codon CCC with CTC, generating the OsOSCA4.1-P450L variant. The mutated sequence was cloned into pCAMBIA1305GFP vector and transformed into Kitaake calli.

ACCEPTED MANUSCRIPT

Downloaded from https://academic.oup.com/plcell/advance-article/doi/10.1093/plcell/koag193/8719692 by National Science & Technology Library user on 03 July 2026

Subcellular localization

To assess the subcellular localization of OsOSCA2.4 and Ososca2.4 in rice, seeds from *Ubi:OsOSCA2.4-GFP/Kitaake*, *Ubi:Ososca2.4-GFP/Kitaake*, *Ubi:OsOSCA2.4-GFP/rab5a* or *Ubi:OsOSCA2.4-GFP/vps9a* transgenic lines were surface-sterilized and cultivated in a culture box with one-half-strength Murashige and Skoog (MS) plus 1% (w/w) agar and 1% (w/w) sucrose at 28°C (12 h light/12 h dark) for 7 days.

To analyze the subcellular localization of OsOSCA2.4 and Ososca2.4 in *N. benthamiana*, the vectors *35S:OsOSCA2.4-GFP* and *35S:Ososca2.4-GFP* were transformed into the EHA105 strain, respectively. The transformed strains were then infiltrated into *N. benthamiana* leaves together with mRFP-tagged markers for 48-72 h.

For heterologous expression in HEK293T cells, the coding sequences of *OsOSCA2.4-GFP* or *Ososca2.4-GFP* were cloned into pmCherry (with *T7* promotor) vector (Matinyan et al. 2021). Plasmids were transfected into HEK293T cells, which were cultured in Dulbecco's modified Eagle's medium (DMEM) supplemented with 10% (v/v) FBS at 37°C with 5% CO_2.

To analyze the subcellular localization of OsOSCA2.4 and Ososca2.4 in the *Xenopus laevis* oocytes, the coding sequences of *OsOSCA2.4-GFP* and *Ososca2.4-GFP* were cloned into the pGEMHE vector (Hou et al, 2014) and transcribed into cRNA using an mMESSAGE mMACHINE T7 kit (Ambion, Austin, TX) following the manufacturer's recommendations. The resulting cRNA were injected into *Xenopus laevis* oocytes, and then incubated in ND96 solution at 18°C for four days before imaging.

To assess the subcellular localization of Rab5a and VPS9a in WT or the *gpa16* mutant, seeds from transgenic lines expressing *Rab5a-GFP* or *VPS9a-GFP* under their respective promoters were surface-sterilized. Then cultivated in a culture box with 1/2 MS plus 1% (w/w) agar and 1% (w/w) sucrose at 28°C (12 h light/12 h dark) for 7 days.

Confocal imaging of *N. benthamiana* leaf cells, rice root tips, rice leaf sheath, HEK293T cells or *Xenopus laevis* oocytes was performed using a Zeiss LS980 with ZEN3.1 software (Zeiss, Germany) laser scanning confocal microscope equipped with a ×20 (NA 1.20) objective lens. The obtained images were analyzed using the Pearson's correlation

ACCEPTED MANUSCRIPT

Downloaded from https://academic.oup.com/plcell/advance-article/doi/10.1093/plcell/koag193/8719692 by National Science & Technology Library user on 03 July 2026

coefficients (PCC) plug-in (Coloc 2) in ImageJ to identify colocalization patterns between the two fluorescently tagged proteins. Additionally, total puncta numbers of Rab5a-GFP and VPS9a-GFP in both WT and *gpa16* were quantified using Adobe Photoshop (http://www.adobe.com).

Cytological observation of rice endosperm

For CBB staining and indirect immunofluorescence analysis, developing endosperm from WT and the *gpa16* mutant were fixed overnight at 4°C in a fixative solution containing 1.25% (v/v) paraformaldehyde, 1.25% (v/v) glutaraldehyde, and 0.1 M PBS (pH 7.2). Fixed samples were subjected to graded dehydration, embedded in resin, and cut into 0.4 μm semithin sections in thickness for CBB staining or indirect immunofluorescence analysis, as described previously (Ren et al. 2020).

For CBB staining, sections were dyed with CBB for 2 min and then decolorized with 10% (v/v) acetic acid. CBB-stained sections were imaged with a Leica DM5000B microscope (Leica, Germany). The ×100 oil immersion objective was used for imaging. The area of PBI or PBII was measured using ImageJ.

For immunofluorescence analysis, sections were initially blocked by Tris-buffered saline containing Tween 20 (TBST) containing 3% (w/v) bovine serum albumin (BSA), followed by incubation with combinations of primary antibodies diluted in TBST containing 1% (w/v) BSA. After three times washes with TBST (BSA free), sections were incubated with Alexa Fluor 488- and 555-conjugated secondary antibodies (Invitrogen), followed by three washes with TBST (BSA free). Primary antibodies against glutelin acidic subunits (1:100) and 13-kD prolamin (1:50) as well as secondary antibodies (1:500) were used. Immunofluorescence-stained sections were imaged with Zeiss LS980 laser scanning confocal microscope (Zeiss, Germany). The ×100 (NA 1.20) oil immersion objective was used for imaging.

For transmission electron microscopy, the developing endosperm was fixed by chemical fixation or high-pressure freezing (EMPACT2, Leica) as described previously (Ren et al. 2020). For immunogold-labeled electron microscopy, developing endosperm was fixed by high-pressure freezing (EM-PACT2, Leica) and freeze substituted with 0.2% (w/v) uranyl

ACCEPTED MANUSCRIPT

Downloaded from https://academic.oup.com/plcell/advance-article/doi/10.1093/plcell/koag193/8719692 by National Science & Technology Library user on 03 July 2026

acetate in acetone at -85°C for 24 h. In an AFS2 automatic freeze substitution unit from Leica, samples were embedded in LOWICRYLHM20 resin by UV light irradiation after a series of gradient dehydration. Ultrathin sections (70 nm in thickness) were prepared with an EM UC7 microtome (Leica). Immunogold labeling on ultrathin sections was performed with primary antibodies (50 mg/mL), followed by incubation with 10-nm or 15-nm gold-conjugated secondary antibodies (1:50; Abcam). An H7700 transmission electron microscope (Hitachi) was used to examine the ultrathin sections after post-staining with aqueous uranyl acetate/lead citrate.

RNA extraction and RT-qPCR Analysis

Total RNA was extracted from various tissues of WT and the *gpa16* mutant using the plant RNA extraction kit (Tiangen). cDNA was reverse transcribed from RNA by a reverse transcription kit (HiScript III; Vazyme). For RT-qPCR, specific primer pairs for *GPA16* (*OsOSCA2.4*), and the internal reference gene *Ubiquitin* (*UBQ*) were shown in Data S1. RT-qPCR analysis was performed using an ABI 7500 RT-qPCR system with the SYBR green mix (Bio-Rad). Relative gene expression levels were calculated using the $2^{-\Delta\Delta Ct}$ method as previously described (Livak and Schmittgen, 2001).

Yeast Two-hybrid (Y2H) Analysis

Y2H analysis was used to detect protein interactions using the DUAL hunter system (Dualsystems Biotech). For the pair studies of Y2H, the coding sequences of target genes were fused to the Cub fragment in pXGY17 vector or the Nub fragment in the pXGY18 vector (Xu et al. 2017), respectively. These constructs were co-transformed into yeast NMY51 using the heat shock method. Positive transformants were selected on synthetic drop-out agar medium -Trp/Leu at 30°C for three days. Protein–protein interactions were further screened on SD medium lacking Ade, His, Trp, and Leu at 30°C for two days. The Y2H assay was carried out using the previously described method (Wang et al. 2021).

Firefly LCI Assays in *N. benthamiana*

The coding sequences of *OsOSCA2.4*, *Ososca2.4*, *Rab5a*, and *VPS9a* were cloned into pCAMBIA-nLUC or pCAMBIA-cLUC vectors (Zhou et al. 2018). All constructed vectors were

ACCEPTED MANUSCRIPT

Downloaded from https://academic.oup.com/plcell/advance-article/doi/10.1093/plcell/koag193/8719692 by National Science & Technology Library user on 03 July 2026

then introduced into EHA105. To assess the self-interaction of OsOSCA2.4, NL-OsOSCA2.4 (*OsOSCA2.4* fused in pCAMBIA-nLUC) and CL-OsOSCA2.4 (*OsOSCA2.4* fused in pCAMBIA-cLUC) were co-infiltrated into *N. benthamiana* leaves. To analyze the interactions of Rab5a with VPS9a coexpressed with OsOSCA2.4 or Ososca2.4, CL-Rab5a and NL-VPS9a were co-infiltrated together with OsOSCA2.4-Flag or Ososca2.4-Flag into *N. benthamiana* leave, respectively. Vectors were expressed in leaves for 48 h to 72 h, and the relative luciferase (LUC) activity was measured using BERTHOLD TECHNOLOGIES Night SHADE LB 985, as previously described.

BiFC Assays in *N. benthamiana*

The coding sequences of *OsOSCA2.4*, *VPS9a* and *GOT1B* were cloned into p2YN vector to generate YN-OsOSCA2.4, YN-VPS9a and YN-GOT1B vectors (Walter et al. 2004), respectively. In parallel, the coding sequences of *OsOSCA2.4*, *Rab5a*, and *Sec23c* were cloned into the p2YC vector to generate YC-OsOSCA2.4, YC-Rab5a, and YC-Sec23c vectors, respectively. The p2YN and p2YC vectors were gifts from Joh A. Lindbo, OARDC, Ohio State University, Wooster. All constructs were introduced into EHA105.

To determine the subcellular site of OsOSCA2.4 self-interaction, YN-OsOSCA2.4 and YC-OsOSCA2.4 were co-infiltrated into *N. benthamiana* leaves along with appropriate organelle markers. To assess the interaction between Rab5a with VPS9a in the presence of OsOSCA2.4 or Ososca2.4, YC-Rab5a, and YN-VPS9a were co-infiltrated into *N. benthamiana* leaves with OsOSCA2.4-Flag or Ososca2.4-Flag, respectively. The interaction of GOT1B and Sec23c was used as a control. Additionally, mCherry was co-infiltrated with each combination to act as a control. Vectors were expressed in leaves for 48 h to 72 h and the fluorescence signals were captured with an LSM980 laser scanning confocal microscope (Zeiss, Germany). The fluorescence intensity was quantified by ZEN3.1, and puncta numbers were counted with Adobe Photoshop software.

Bioinformatic analyses

Homologs of rice OsOSCA2.4 in rice and *Arabidopsis* were identified using the BLASTP search program of the National Center for Biotechnology Information (http://www.

ACCEPTED MANUSCRIPT

Downloaded from https://academic.oup.com/plcell/advance-article/doi/10.1093/plcell/koag193/8719692 by National Science & Technology Library user on 03 July 2026

ncbi.nlm.nih.gov). Phylogenetic analyses were conducted with MEGA12.0 (http://www.megasoftware.net), based on the neighbor-joining method with the following parameters: p-distance method, pairwise deletion, and bootstrap (500 replicates; random seed). Topology prediction for OsOSCA2.4 was deduced using AlphaFold (https://alphafold.com) and PyMOL (https://www.pymol.org).

Co-IP assays in *N. benthamiana*

Proteins in transformed leaves of *N. benthamiana* were extracted as described above. The filtered homogenate was incubated with GFP beads (ChromoTek) at 4°C in a top-to-end rotator for 1 h followed by 4 times washing. Then, the samples were boiled after adding 5× protein loading buffer for immunoblot analyses.

Analysis of Ca^{2+} levels in cytosol, PVC, and TGN in rice protoplasts

To target the fluorescence resonance energy transfer (FRET)-based Ca^{2+} biosensor YC3.6 to specific subcellular compartments, the *PRpHluorin* sequence in pBI221-PRpHluorin-AtVSR2TMDCT and pBI221-PRpHluorin-BP80Y612A were replaced by the coding sequence of *YC3.6*, resulting in the generation of vectors pBI221-YC3.6-AtVSR2TMDCT (YC3.6-PVC) and pBI221-YC3.6-BP80(Y612A) (YC3.6-TGN), respectively (Nagai et al. 2004; Shen et al. 2013). The PRpHluorin-related vectors were kind gifts from Dr. JB. Shen. Concurrently, the coding sequence of *YC3.6* was inserted into pBI221 to generate the vector pBI221-YC3.6-CYT, which localized to the cytosol.

All constructed vectors were coexpressed with organelle markers in rice protoplasts to confirm subcellular targeting. For Ca^{2+} measurements, protoplasts were prepared from 10-day-old seedlings of WT and *gpa16* grown in the darkness at 28°C. YC3.6-PVC, YC3.6-TGN, and YC3.6-CYT were expressed in protoplasts for 16 h at 25°C. A Zeiss LSM980 laser scanning confocal microscope with the ×20 (NA 1.20) objective (Zeiss, Germany) was used to capture the images. YC3.6 fluorescence was excited with the 458 nm. The CFP emission was collected at the wavelength from 465-505 nm, and FRET-dependent Venus emission (YFP) was collected between 520-540 nm. To ensure data reliability, the acquisition

ACCEPTED MANUSCRIPT

Downloaded from https://academic.oup.com/plcell/advance-article/doi/10.1093/plcell/koag193/8719692 by National Science & Technology Library user on 03 July 2026

parameters for all samples were kept constant throughout a single experimental replicate. CFP and YFP intensity were analyzed by ZEN3.1.

To target the Ca^{2+} biosensor GCaMP6s to the outer surface of the PVC, the *GCaMP6s* sequence was fused with 2×FYVE and with mCharry linked by 2A peptide. The fused sequence was cloned into the pAN580 vector (Ren et al. 2020). For Ca^{2+} measurements, protoplasts were prepared from 10-day-old seedlings of WT and *gpa16* grown in the darkness at 28°C. The constructed vector was expressed in rice protoplasts for 16 h at 25°C. A Zeiss LSM980 laser scanning confocal microscope with the ×20 (NA 1.20) objective (Zeiss, Germany) was used to capture the images. To ensure data reliability, the acquisition parameters for all samples were kept constant throughout a single experimental replicate. GFP and mCherry intensity were analyzed by ZEN3.1.

Ca^{2+} imaging assays

PM-localized OsOSCA2.4-LV-AA and Ososca2.4-LV-AA variants were obtained by mutation of two LL-motifs of OsOSCA2.4 (Ososca2.4) into LV or AA.

For Ca^{2+} imaging, the mutated DNA fragment was inserted into the binary vector pCAMBIA1305GFP (remove the GFP fragment by enzyme digestion) and then coexpressed with GCaMP6s in *N. benthamiana* for 48h to 72 h. Leaf tissue was cut into small pieces and put into a 96-well black flat-bottom Corning assay plate containing 150 µl 1/2 MS. Samples were incubated in the dark for 2 h to stabilize Ca^{2+} level. GCaMP6s fluorescence was recorded at 30-second intervals with a multimode microplate reader (Varioskan LUX; Thermo Scientific), until the baseline stable. Next, the medium was replaced by 1/2 MS supplemented with 1 mM βCD (MCE, HY-107201), followed by recording for additional 40 cycles at 30-second intervals. Emission intensity was collected at 520 nm with excitation light at 480 nm.

Ca^{2+} related chemical treatments

For ionomycin- and EGTA-related assays, leaves of *N. benthamiana* expressing the 35S-promoted GCaMP6s Ca^{2+} biosensor, GFP or BiFC vectors (YC-Rab5a and YN-VPS9a) were

ACCEPTED MANUSCRIPT

Downloaded from https://academic.oup.com/plcell/advance-article/doi/10.1093/plcell/koag193/8719692 by National Science & Technology Library user on 03 July 2026

secured with scotch tape to the glass-bottomed petri dish (Cellvis, D35-14-1-N), with the upper leaf surface facing the glass slide. Samples were covered with liquid 1/2 MS. For imaging, DMSO or ionomycin (Merck Millipore) plus EGTA were injected to the dish. The final concentration of ionomycin was maintained at 10 μM, and the final concentration of EGTA was kept at 10 mM. Subsequently, images were captured in time-lapse mode for 240s with a frame rate of 3s. GFP was used as a control. Fluorescence intensities of YFP (BiFC), GFP and GCaMP6s were analyzed with ZEN3.1 software.

For EGTA-AM-related assays, Rab5a-GFP or VPS9a-GFP transgenic seeds were surface sterilized and cultivated on 1/2 MS supplemented with 1% (w/w) agar and 1% (w/w) sucrose at 28°C (12 h light/12 h dark) for 7 days. Then roots of seedlings were treated with liquid 1/2 MS containing either DMSO or 10 μM EGTA-AM (Merck Millipore) for 2 h. Images were acquired using a Zeiss LS980 laser scanning confocal microscope with a ×20 objective lens (NA 1.20). The total puncta number of Rab5a-GFP or VPS9a-GFP were quantified with Adobe Photoshop (http://www.adobe.com).

Xenopus laevis oocytes electrophysiology

The coding sequences of *OsOSCA2.4*, *Ososca2.4*, *CNGC2*, and *CNGC4* were inserted into the pGEMHE vector and transcribed into cRNA using an mMESSAGE mMACHINE T7 kit (Ambion, Austin, TX). The cRNA was injected into *Xenopus laevis* oocytes and incubated in ND96 solution at 18°C for 4 days. The oocytes electrophysiological analysis procedure followed the guidelines as previously described (Hou et al. 2014). In brief, oocytes were voltage-clamped at potential of –60 mV (for hyperosmotic stimuli) or –140-40 mV (for voltage stimuli) using a TEV 200 amplifier (Dagan, Minneapolis, MN) and monitored by computer through a Digidata 1440A/D converter and pCLAMP 10.2 software (Axon Instruments, Foster City, CA). The pipette solution contained 3 M KCl. The oocytes were perfused with a standard ND96 solution containing 96 mM NaCl, 2.0 mM KCl, 1.0 mM $MgCl_2$, 20 mM $CaCl_2$, and 10 mM HEPES, pH 7.5, at room temperature. Hyperosmotic stimulation was achieved by perfusing the oocytes with a bath solution containing the indicated concentrations of mannitol.

Statistical analysis

ACCEPTED MANUSCRIPT

Downloaded from https://academic.oup.com/plcell/advance-article/doi/10.1093/plcell/koag193/8719692 by National Science & Technology Library user on 03 July 2026

Source data for all quantitative and statistical analyses are provided in Data S2 in the Supplementary Materials. Comparisons are made by two-tailed Student's *t* test. Statistical analyses and figure preparation were performed using GraphPad Prism 9.0 (GraphPad Software), ImageJ and Python 3.12.4. Pearson's correlation coefficients (PCC) were calculated by plug-in (Coloc 2) in ImageJ. For Ca^{2+} imaging assays, fluorescence intensities or FRET ratios were quantified by SkanIt 7.1 or ZEN 3.1 software. The sample size (*n*), statistical tests used, and exact P values are indicated in the corresponding figure legends. Differences were considered statistically significant at $P < 0.05$.

Accession numbers

Sequence data from this article can be found in the GenBank/EMBL libraries with the following accession numbers: *OsOSCA2.4* (*Os12g0583800*), *Rab5a* (*Os12g0631100*), *VPS9a* (*Os03g0262900*), *GOT1B* (*Os03g0209400*), *Sec23c* (*Os11g0433500*), *VAMP727* (*Os08g0558600*), *OsOSCA1.1* (*Os01g0534900*), *OsOSCA1.2* (*Os05g0594700*), *OsOSCA1.3* (*Os05g0393800*), *OsOSCA1.4* (*Os10g0579100*), *OsOSCA2.1* (*Os12g0633600*), *OsOSCA2.2* (*Os03g0673800*), *OsOSCA2.3* (*Os03g0726300*), *OsOSCA2.5* (*Os01g0950900*), *OsOSCA3.1* (*Os07g0150100*), *OsOSCA4.1* (*Os03g0137400*), *CNGC2* (*At5g15410*), *CNGC4* (*At5g54250*), *AtOSCA1.1* (*At4g04340*), *AtOSCA1.2* (*At4g22120*), *AtOSCA1.3* (*At1g11960*), *AtOSCA1.4* (*At1g62320*), *AtOSCA1.5* (*At3g21620*), *AtOSCA1.6* (*At4g15430*), *AtOSCA1.7* (*At4g02900*), *AtOSCA1.8* (*At1g32090*), *AtOSCA2.1* (*At1g58520*), *AtOSCA2.2* (*At1g10090*), *AtOSCA2.3* (*At3g01100*), *AtOSCA2.4* (*At1g69450*), *AtOSCA2.5* (*At3g54510*), *AtOSCA3.1* (*At1g30360*), *AtOSCA4.1* (*At4g35870*).

Acknowledgments

We thank for the Core Facility Platform, Institute of Crop Sciences, Chinese Academy of Agricultural Sciences, for their assistance with confocal imaging and transmission electron microscopy analysis. We thank for Jiangsu Nanjing Rice Germplasm Resources National Field Observation and Research Station. We also thank Inner Mongolia Innovation Center of Biological Breeding Technology. The CRISPR/Cas9 vector was kindly provided by Yunde Zhao

ACCEPTED MANUSCRIPT

Downloaded from https://academic.oup.com/plcell/advance-article/doi/10.1093/plcell/koag193/8719692 by National Science & Technology Library user on 03 July 2026

(University of California, San Diego). The pGEMHE vector was generously provided by Legong Li (Capital Normal University).

Funding

National Key Research and Development Program of China (2021YFF1000200); National Natural Science Foundation of China (31830064 and 32172085); Basic Research Center, Innovation Program of Chinese Academy of Agricultural Sciences (CAAS-CSNCB-202302); Central Public-interest Scientific Institution Basal Research Fund (S2024ZD01); China Agriculture Research System (CARS-01-05)

Author Contributions

Jianmin Wan and Yulong Ren supervised the project. Y.Z. Yun Zhu, and P.Z. performed all experiments and analyzed data. W.T. H.D. Z.L. Y.C. X.B. T.P. Y.X. X.W. Z.R. X.J. X.H. R.J. H.W. C.G. R.C. X.C. J.L. E.D. C.L. Z.C. J.W. and Y.B. provided critical technical support. Jianmin Wan, Yulong Ren, Yihua Wang, Haiyang Wang, and Chuanyin Wu wrote the paper.

Declaration of interests:

The authors declare no competing interests.

Data and materials availability

All data needed to evaluate and reproduce the results in the paper are present in the paper and/or the Supplementary Materials.

References

Antebi A and Fink GR. 1992. The yeast Ca^{2+}-ATPase homologue, PMR1, is required for normal Golgi function and localizes in a novel Golgi-like distribution. Mol Biol Cell. **3**:633–654. https://doi.org/10.1091/mbc.3.6.633

Ashnest JR, Huynh DL, Dragwidge JM, Ford BA, and Gendall AR. 2015. *Arabidopsis* intracellular NHX-type sodium-proton antiporters are required for seed storage protein processing. Plant Cell Physiol. **56**:2220–2233. https://doi.org/10.1093/pcp/pcv138

ACCEPTED MANUSCRIPT

Downloaded from https://academic.oup.com/plcell/advance-article/doi/10.1093/plcell/koag193/8719692 by National Science & Technology Library user on 03 July 2026

Bao X, et al. 2023. A deleterious *Sar1c* variant in rice inhibits export of seed storage proteins from the endoplasmic reticulum. Plant Mol Biol. **111**:307. https://doi.org/10.1007/s11103-022-01327-z

Bonifacino JS and Glick BS. 2004. The mechanisms of vesicle budding and fusion. Cell. **116**:153–166. https://doi.org/10.1016/s0092-8674(03)01079-1

Chen T, et al. 2013. Ultra-sensitive fluorescent proteins for imaging neuronal activity. Nature. **499**:295–300. https://doi.org/10.1038/nature12354

Cox CD, Zhang Y, Zhou Z, Walz T, and Martinac B. 2021. Cyclodextrins increase membrane tension and are universal activators of mechanosensitive channels. Proc Natl Acad Sci USA. **118**:1–12. https://doi.org/doi.org/10.1073/pnas.2104820118

Deng Y, et al. 2018. Activity of the SPCA1 calcium pump couples sphingomyelin synthesis to sorting of secretory proteins in the *trans*-Golgi network. Dev Cell. **47**:464–478. https://doi.org/10.1016/j.devcel.2018.10.012

D'hooge P, et al. 2015. Ca^{2+} homeostasis in the budding yeast *Saccharomyces cerevisiae*: Impact of ER/Golgi Ca^{2+} storage. Cell Calcium. **58**:226–235. https://doi.org/10.1016/j.ceca.2015.05.004

Ding X, et al. 2022. Microautophagy mediates vacuolar delivery of storage proteins in maize aleurone cells. Front Plant Sci. **18**:833612. https://doi.org/10.3389/fpls.2022.833612

Fukuda M, et al. 2011. The small GTPase Rab5a is essential for intracellular transport of proglutelin from the Golgi apparatus to the protein storage vacuole and endosomal membrane organization in developing rice endosperm. Plant Physiol. **157**:632–644. https://doi.org/10.1104/pp.111.180505

Gao C, et al. 2014. A Unique plant ESCRT component, FREE1, regulates multivesicular body protein sorting and plant growth. Curr Biol. **24**:2556–2563. https://doi.org/10.1016/j.cub.2014.09.014

Goh T, et al. 2007. VPS9a, the common activator for two distinct types of Rab5 GTPases, is essential for the development of *Arabidopsis thaliana*. Plant Cell. **19**:3504–3515. https://doi.org/10.1105/tpc.107.053876

Guichard M, Thomine S, and Frachisse JM. 2022. Mechanotransduction in the spotlight of mechano-sensitive channels. Curr Opin Plant Biol. **68**:102252. https://doi.org/10.1016/j.pbi.2022.102252

Han Y, et al. 2024. Mechanical activation opens a lipid-lined pore in OSCA ion channels. Nature. **628**:910–918. https://doi.org/10.1038/s41586-024-07256-9

Hay JC. 2007. Calcium: a fundamental regulator of intracellular membrane fusion? EMBO Rep. **8**:236–240. https://doi.org/10.1038/sj.embor.7400921

ACCEPTED MANUSCRIPT

Downloaded from https://academic.oup.com/plcell/advance-article/doi/10.1093/plcell/koag193/8719692 by National Science & Technology Library user on 03 July 2026

He W, Wang L, Lin QL, and Yu F. 2021. Rice seed storage proteins: Biosynthetic pathways and the effects of environmental factors. J Integr Plant Biol. **63**:1999–2019. https://doi.org/10.1111/jipb.13176

Heath JD, Weldon R, Monnot C, and Meinke DW. 1986. Analysis of storage proteins in normal and aborted seeds from embryo-lethal mutants of *Arabidopsis thaliana*. Planta. **169**:304–312. https://doi.org/Doi%252010.1007/Bf00392124

Hedrich R. 2012. Ion channels in plants. Physiol Rev. **92**:1777–1811. https://doi.org/10.1152/physrev.00038.2011

Hou C, et al. 2014. DUF221 proteins are a family of osmosensitive calcium-permeable cation channels conserved across eukaryotes. Cell Res. **24**:632–635. https://doi.org/10.1038/cr.2014.14

Hu M, et al. 2024. The ion channels of endomembranes. Physiol Rev. **104**:1335–1385. https://doi.org/10.1152/physrev.00025.2023

Jojoa-Cruz S, et al. 2018. Cryo-EM structure of the mechanically activated ion channel OSCA1.2. Elife. **7**:1–17. https://doi.org/10.7554/eLife.41845

Jojoa-Cruz S, Burendei B, Lee WH, and Ward AB. 2024. Structure of mechanically activated ion channel OSCA2.3 reveals mobile elements in the transmembrane domain. Structure. **32**:157–167. https://doi.org/10.1016/j.str.2023.11.009

Thor K, et al. 2020. The calcium-permeable channel OSCA1.3 regulates plant stomatal immunity. Nature. **585**:569–573. https://doi.org/10.1038/s41586-020-2702-1

Kawakatsu T, Hirose S, Yasuda H, and Takaiwa F. 2010. Reducing rice seed storage protein accumulation leads to changes in nutrient quality and storage organelle formation. Plant Physiol. **154**:1842–1854. https://doi.org/10.1104/pp.110.164343

Kilpatrick BS, Eden ER, Schapira AH, Futter CE, and Patel S. 2013. Direct mobilisation of lysosomal Ca^{2+} triggers complex Ca^{2+} signals. J Cell Sci. **126**:60–66. https://doi.org/10.1242/jcs.118836

Kleczkowski LA, Kunz S, and Wilczynska M. 2010. Mechanisms of UDP-Glucose synthesis in plants. Crit Rev Plant Sci. **29**:191–203. https://doi.org/10.1080/07352689.2010.483578

Kumamaru T, et al. 2010. Vacuolar processing enzyme plays an essential role in the crystalline structure of glutelin in rice seed. Plant Cell Physiol. **51**:38–46. https://doi.org/10.1093/pcp/pcp165

Langemeyer L, Fröhlich F, and Ungermann C. 2018. Rab GTPase function in endosome and lysosome biogenesis. Trends Cell Biol. **28**:957–970. https://doi.org/10.1016/j.tcb.2018.06.007

ACCEPTED MANUSCRIPT

Downloaded from https://academic.oup.com/plcell/advance-article/doi/10.1093/plcell/koag193/8719692 by National Science & Technology Library user on 03 July 2026

Lelouvier B and Puertollano R. 2011. Mucolipin-3 regulates luminal calcium, acidification, and membrane fusion in the endosomal pathway. J Biol Chem. **286**:9826–9832. https://doi.org/10.1074/jbc.M110.169185

Liu F, et al. 2013. OsVPS9a functions cooperatively with OsRab5a to regulate post-Golgi dense vesicle-mediated storage protein trafficking to the protein storage vacuole in rice endosperm cells. Mol Plant. **6**:1918–1932. https://doi.org/10.1093/MP/SST081

Liu X, Wang J, and Sun L. 2018. Structure of the hyperosmolality-gated calcium-permeable channel OSCA1.2. Nat Commun. **9**:50–60. https://doi.org/10.1038/s41467-018-07564-5

Livak KJ and Schmittgen TD. 2001. Analysis of relative gene expression data using real-time quantitative PCR and the $2^{-\Delta\Delta CT}$ method. Methods. **25**:402–408. https://doi.org/10.1006/meth.2001.1262

Maity K, et al. 2019. Cryo-EM structure of OSCA1.2 from *Oryza sativa* elucidates the mechanical basis of potential membrane hyperosmolality gating. Proc Natl Acad Sci USA. **116**:14309–14318. https://doi.org/10.1073/pnas.1900774116

Matinyan N, et al. 2021. Multiplexed drug-based selection and counterselection genetic manipulations in *Drosophila*. Cell Reports. **36**:109700. https://doi.org/10.1016/j.celrep.2021.109700

Miao Y, Yan PK, Kim H, Hwang I, and Jiang L. 2006. Localization of green fluorescent protein fusions with the seven *Arabidopsis* vacuolar sorting receptors to prevacuolar compartments in tobacco BY-2 cells. Plant Physiol. **142**:945–962. https://doi.org/10.1104/pp.106.083618

Murthy SE, et al. 2018. OSCA/TMEM63 are an evolutionarily conserved family of mechanically activated ion channels. Elife. **7**:1–17. https://doi.org/10.7554/eLife.41844

Nagai T, Yamada S, Tominaga T, Ichikawa M, and Miyawaki A. 2004. Expanded dynamic range of fluorescent indicators for Ca^{2+} by circularly permuted yellow fluorescent proteins. Proc Natl Acad Sci USA. **101**:10554–10559. https://doi.org/10.1073/pnas.0400417101

Nebenführ A, et al. 1999. Stop-and-go movements of plant Golgi stacks are mediated by the acto-myosin system. Plant Physiol. **121**:1127–1142. https://doi.org/10.1104/pp.121.4.1127

Niu J, et al. 2025. Rice-derived recombinant human serum albumin as an alternative to human plasma for patients with decompensated liver cirrhosis: a randomised, double-blind, positive-controlled and non-inferiority trial. Gut. **74**:1476–1485. https://doi.org/10.1136/gutjnl-2025-335577

Osborne TB. 1924. The vegetable proteins. Nature. **114**:822. https://doi.org/10.1038/114822c0

Otegui MS, Herder R, Schulze J, Jung R, and Staehelin LA. 2006. The proteolytic processing of seed storage proteins in *Arabidopsis* embryo cells starts in the multivesicular bodies. Plant Cell. **18**:2567–2581. https://doi.org/10.1105/tpc.106.040931

ACCEPTED MANUSCRIPT

Downloaded from https://academic.oup.com/plcell/advance-article/doi/10.1093/plcell/koag193/8719692 by National Science & Technology Library user on 03 July 2026

Pan T, et al. 2021. Post-Golgi trafficking of rice storage proteins requires the small GTPase Rab7 activation complex MON1–CCZ1. Plant Physiol. **184**:2174–2176. https://doi.org/10.1093/plphys/kiab175

Parkinson K, et al. 2014. Calcium-dependent regulation of Rab activation and vesicle fusion by an intracellular P2X ion channel. Nat Cell Biol. **16**:87–98. https://doi.org/10.1038/ncb2887

Pei S, et al. 2024. Osmosensor-mediated control of Ca^{2+} spiking in pollen germination. Nature. **629**:1118–1125. https://doi.org/10.1038/s41586-024-07445-6

Reguera M, et al. 2015. Ph regulation by NHX-type antiporters is required for receptor-mediated protein trafficking to the vacuole in *Arabidopsis*. Plant Cell. **27**:1200–1217. https://doi.org/10.1105/tpc.114.135699

Ren Y, et al. 2014. *GLUTELIN PRECURSOR ACCUMULATION3* encodes a regulator of post-Golgi vesicular traffic essential for vacuolar protein sorting in rice endosperm. Plant Cell. **26**:410–425. https://doi.org/10.1105/tpc.113.121376

Ren Y, et al. 2020. *GPA5* encodes a Rab5a effector required for post-Golgi trafficking of rice storage proteins. Plant Cell. **32**:758–777. https://doi.org/10.1105/tpc.19.00863

Ren Y, et al. 2022. Endomembrane-mediated storage protein trafficking in plants: Golgi-dependent or Golgi-independent? FEBS Lett. **596**:2215–2230. https://doi.org/10.1002/1873-3468.14374

Reyes FC, et al. 2011. Delivery of prolamins to the protein storage vacuole in maize aleurone cells. Plant Cell. **23**:769–784. https://doi.org/10.1105/tpc.110.082156

Ruan H, Wang T, Ren H, and Zhang Y. 2023. AtFH5-labeled secretory vesicles-dependent calcium oscillation drives exocytosis and stepwise bulge during pollen germination. Cell Rep. **42**:113319. https://doi.org/10.1016/j.celrep.2023.113319

Sanderfoot AA, Kovaleva V, Bassham DC, and Raikhel NV. 2001. Interactions between syntaxins identify at least five SNARE complexes within the Golgi/prevacuolar system of the *Arabidopsis* cell. Mol Biol Cell. **12**:3733–3743. https://doi.org/10.1091/mbc.12.12.3733

Shen J, et al. 2013. Organelle pH in the *Arabidopsis* endomembrane system. Mol. Plant. **6**:1419–1437. https://doi.org/10.1093/mp/sst079

Shewry PR, Napier JA, and Tatham AS. 1995. Seed storage proteins: Structures and biosynthesis. Plant Cell. **7**:945–956. https://doi.org/10.2307/3870049

Südhof TC. 2013. A molecular machine for neurotransmitter release: synaptotagmin and beyond. Nat Med. **19**:1227–1231. https://doi.org/10.1038/nm.3338

ACCEPTED MANUSCRIPT

Downloaded from https://academic.oup.com/plcell/advance-article/doi/10.1093/plcell/koag193/8719692 by National Science & Technology Library user on 03 July 2026

Szymczak AL, et al. 2004. Correction of multi-gene deficiency in vivo using a single "self-cleaving" 2A peptide–based retroviral vector. Nat Biotechnol. **22**:589–594. https://doi.org/10.1038/nbt957

Takahashi H, et al. 2004. Differential localization of tonoplast intrinsic proteins on the membrane of protein body type II and aleurone grain in rice seeds. Biosci Biotechnol Biochem. **68**:1728–1736. https://doi.org/10.1271/bbb.68.1728

Takahashi H, et al. 2005. A novel vesicle derived directly from endoplasmic reticulum is involved in the transport of vacuolar storage proteins in rice endosperm. Plant Cell Physiol. **46**:245–249. https://doi.org/10.1093/pcp/pci019

Takaiwa F, Wakasa Y, Hayashi S, and Kawakatsu T. 2017. An overview on the strategies to exploit rice endosperm as production platform for biopharmaceuticals. Plant Sci. **263**:201–209. https://doi.org/10.1016/j.plantsci.2017.07.016

Takemoto K, et al. 2018. Distinct sets of tethering complexes, SNARE complexes, and Rab GTPases mediate membrane fusion at the vacuole in *Arabidopsis*. Proc Natl Acad Sci USA. **115**:E2457–E2466. https://doi.org/10.1073/pnas.1717839115

Takemoto Y, et al. 2002. The rice mutant *esp2* greatly accumulates the glutelin precursor and deletes the protein disulfide isomerase. Plant Physiol. **128**:1212–1222. https://doi.org/10.1104/pp.010624

Tian W, et al. 2019. A calmodulin-gated calcium channel links pathogen patterns to plant immunity. Nature. **572**:131–135. https://doi.org/10.1038/s41586-019-1413-y

Ueda Y, et al. 2010. Gene-gene interactions between mutants that accumulate abnormally high amounts of proglutelin in rice seed. Breed Sci. **60**:568–574. https://doi.org/10.1270/jsbbs.60.568

Schmidt U, et al. 2006. Endocytosis of the glucose transporter GLUT8 is mediated by interaction of a dileucine motif with the β2-adaptin subunit of the AP-2 adaptor complex. J Cell Sci. **119**:2321–2331. https://doi.org/10.1242/jcs.02943

Walter M, et al. 2004. Visualization of protein interactions in living plant cells using bimolecular fluorescence complementation. Plant J. **40**:428–438. https://doi.org/10.1111/j.1365-313X.2004.02219.x

Wang Y, et al. 2009. The vacuolar processing enzyme OsVPE1 is required for efficient glutelin processing in rice. Plant J. **58**:606–617. https://doi.org/10.1111/j.1365-313X.2009.03801.x

Wang Y, et al. 2010. OsRab5a regulates endomembrane organization and storage protein trafficking in rice endosperm cells. Plant J. **64**:812–824. https://doi.org/10.1111/j.1365-313X.2010.04370.x

ACCEPTED MANUSCRIPT

Downloaded from https://academic.oup.com/plcell/advance-article/doi/10.1093/plcell/koag193/8719692 by National Science & Technology Library user on 03 July 2026

Wang Y, et al. 2016. GOLGI TRANSPORT 1B regulates protein export from the endoplasmic reticulum in rice endosperm cells. Plant Cell. **28**:2850–2865. https://doi.org/10.1105/tpc.16.00717

Wang J, et al. 2021. Transcriptional activation and phosphorylation of OsCNGC9 confer enhanced chilling tolerance in rice. Mol. plant. **14**:315–329. https://doi.org/10.1016/j.molp.2020.11.022

Wen L, et al. 2015. Guanine nucleotide exchange factor 2 for Rab5 proteins coordinated with GLUP6/GEF regulates the intracellular transport of the proglutelin from the Golgi apparatus to the protein storage vacuole in rice endosperm. J Exp Bot. **66**:6137–6147. https://doi.org/10.1093/jxb/erv325

Woll KA and Van Petegem F. 2022. Calcium-release channels: structure and function of IP(3) receptors and ryanodine receptors. Physiol Rev. **102**:209–268. https://doi.org/10.1152/physrev.00033.2020

Xu Y, et al. 2017. OsCNGC13 promotes seed-setting rate by facilitating pollen tube growth in stylar tissues. PLOS Genet. **13**:e1006906. https://doi.org/10.1371/journal.pgen.1006906

Yau KW. 1994. Cyclic nucleotide-gated channels: an expanding new family of ion channels. Proc Natl Acad Sci USA. **91**:3481–3483. https://doi.org/10.1073/pnas.91.9.3481

Yuan F, et al. 2014. OSCA1 mediates osmotic-stress-evoked Ca^{2+} increases vital for osmosensing in *Arabidopsis*. Nature. **514**:367–371. https://doi.org/10.1038/nature13593

Zhang M, Shan Y, Cox CD, and Pei D. 2023. A mechanical-coupling mechanism in OSCA/TMEM63 channel mechanosensitivity. Nat Commun. **14**:1–9. https://doi.org/10.1038/s41467-023-39688-8

Zhang M, et al. 2018. Structure of the mechanosensitive OSCA channels. Nat Struct Mol Biol. **25**:850–858. https://doi.org/10.1038/s41594-018-0117-6

Zheng P, Zheng C, Otegui MS, and Li F. 2022a. Endomembrane mediated-trafficking of seed storage proteins: from *Arabidopsis* to cereal crops. J Exp Bot. **73**:1312–1326. https://doi.org/10.1093/jxb/erab519

Zheng Q, et al. 2022b. Calcium transients on the ER surface trigger liquid-liquid phase separation of FIP200 to specify autophagosome initiation sites. Cell. **185**:4082–4098. https://doi.org/10.1016/j.cell.2022.09.001

Zhou Z, Bi G, and Zhou J. 2018. Luciferase complementation assay for protein-protein interactions in plants. Curr Protoc Plant Biol. **3**:42–50. https://doi.org/10.1002/cppb.20066

Zhu J, et al. 2019. OsNHX5-mediated pH homeostasis is required for post-Golgi trafficking of seed storage proteins in rice endosperm cells. BMC Plant Biol. **19**:295–306. https://doi.org/10.1186/s12870-019-1911-y

ACCEPTED MANUSCRIPT

Downloaded from https://academic.oup.com/plcell/advance-article/doi/10.1093/plcell/koag193/8719692 by National Science & Technology Library user on 03 July 2026

Zhu J, et al. 2021. Subunit E isoform 1 of vacuolar H$^+$-ATPase OsVHA enables post-Golgi trafficking of rice seed storage proteins. Plant Physiol. **187**:2192–2208. https://doi.org/10.1093/plphys/kiab099

Figures and Tables

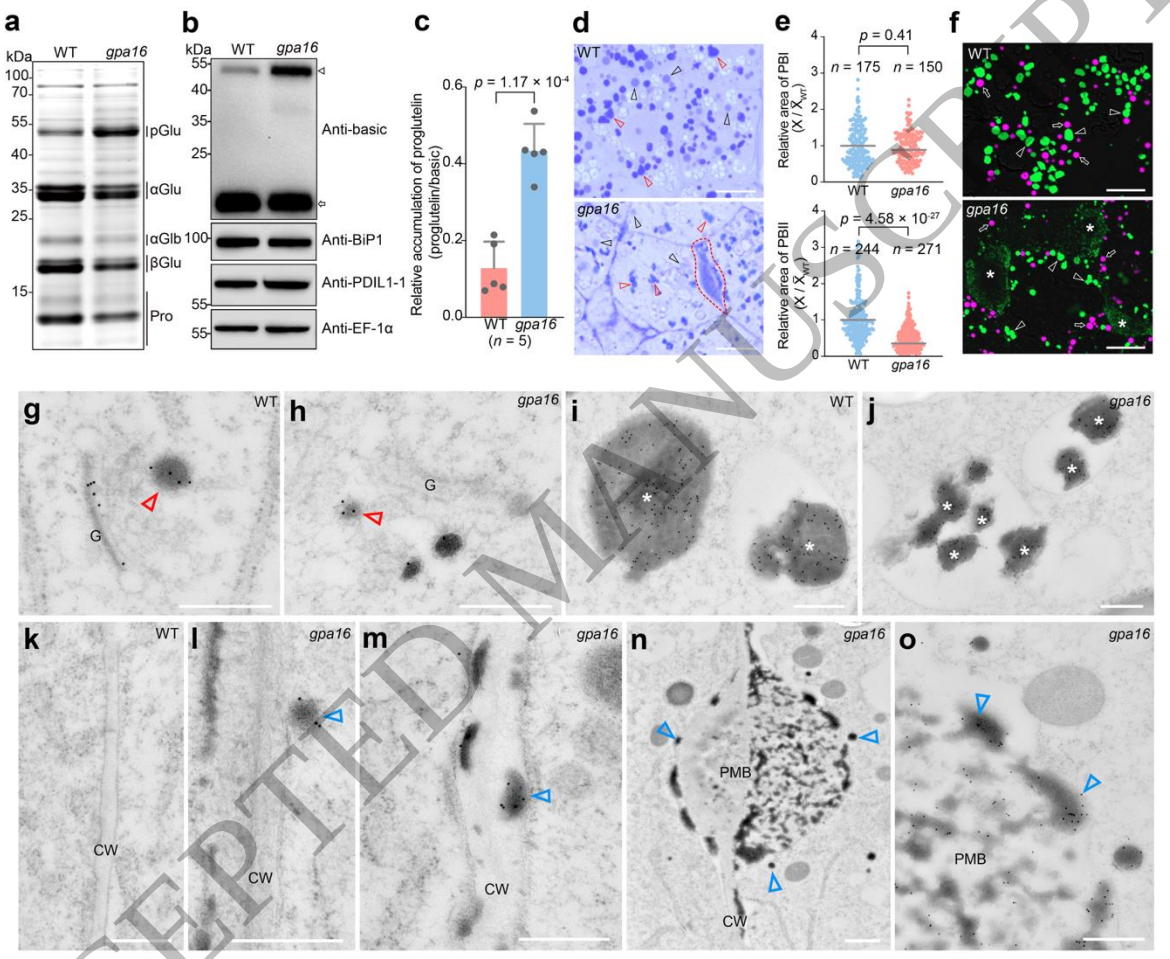

Figure 1. Phenotypic characterization of the *gpa16* mutant.

(**a**) Total SSP profiles of WT and *gpa16* mature seeds on an SDS-PAGE gel stained with CBB. Molecular weight markers are shown on the left (kDa). pGlu, proglutelins; αGlu, glutelin acidic subunits; αGlb, α-globulin; βGlu, glutelin basic subunits; Pro, prolamins. (**b**) Immunoblot analysis of WT and *gpa16* mature seeds using antibodies against glutelin basic subunits, BiP1 and PDIL1-1. EF-1α serves as a loading control. Arrowhead indicates the proglutelins, arrow indicates glutelin basic subunits. (**c**) Quantification of relative proglutelin accumulation level in WT and *gpa16* in (**b**). (**d**) Light microscopy images of CBB-stained semi-thin sections from developing WT and *gpa16* endosperm. Black and red arrowheads

ACCEPTED MANUSCRIPT

Downloaded from https://academic.oup.com/plcell/advance-article/doi/10.1093/plcell/koag193/8719692 by National Science & Technology Library user on 03 July 2026

indicate PBIs and PBIIs, respectively. The red dotted line outlines the PMB. Scale bars, 10 μm. (**e**) Quantitative analyses of PBI and PBII relative areas in WT and *gpa16* in (**d**). X indicates the area of PBI or PBII, and $\overline{X}_{WT}$ indicates the mean value in WT. Individual data points and means are shown. Gray lines represent the mean values. (**f**) Immunofluorescence images of glutelins (green) and prolamins (red) in subaleurone cells of WT and *gpa16*. White arrowheads indicate PBIIs; white arrows and asterisks indicate PBIs and glutelin-containing PMBs, respectively. Scale bars, 10 μm. (**g-o**) Immunogold labeling of glutelins depicting the possible origin and formation of the PMBs. (**g**, **h**), DVs (red arrowheads) bud from the Golgi in both WT (**g**) and *gpa16* (**h**). (**i**, **j**) Glutelins (wight asterisks) distribution in the PSV of WT (**i**) and *gpa16* (**j**) endosperm. (**k-o**) The cell wall (CW) structures of WT (**k**) and *gpa16* (**l-o**) endosperm. DVs were mis-sorted (blue arrowheads) to cell periphery (**l**) and discharged their contents into the apoplast space in *gpa16* (**l-o**). Scale bars, 500 nm in (**g**-**m**, **o**), 1 μm in (**n**). In (**c**, **e**), statistical analyses were performed by two-tailed Student's *t* test.

ACCEPTED MANUSCRIPT

Downloaded from https://academic.oup.com/plcell/advance-article/doi/10.1093/plcell/koag193/8719692 by National Science & Technology Library user on 03 July 2026

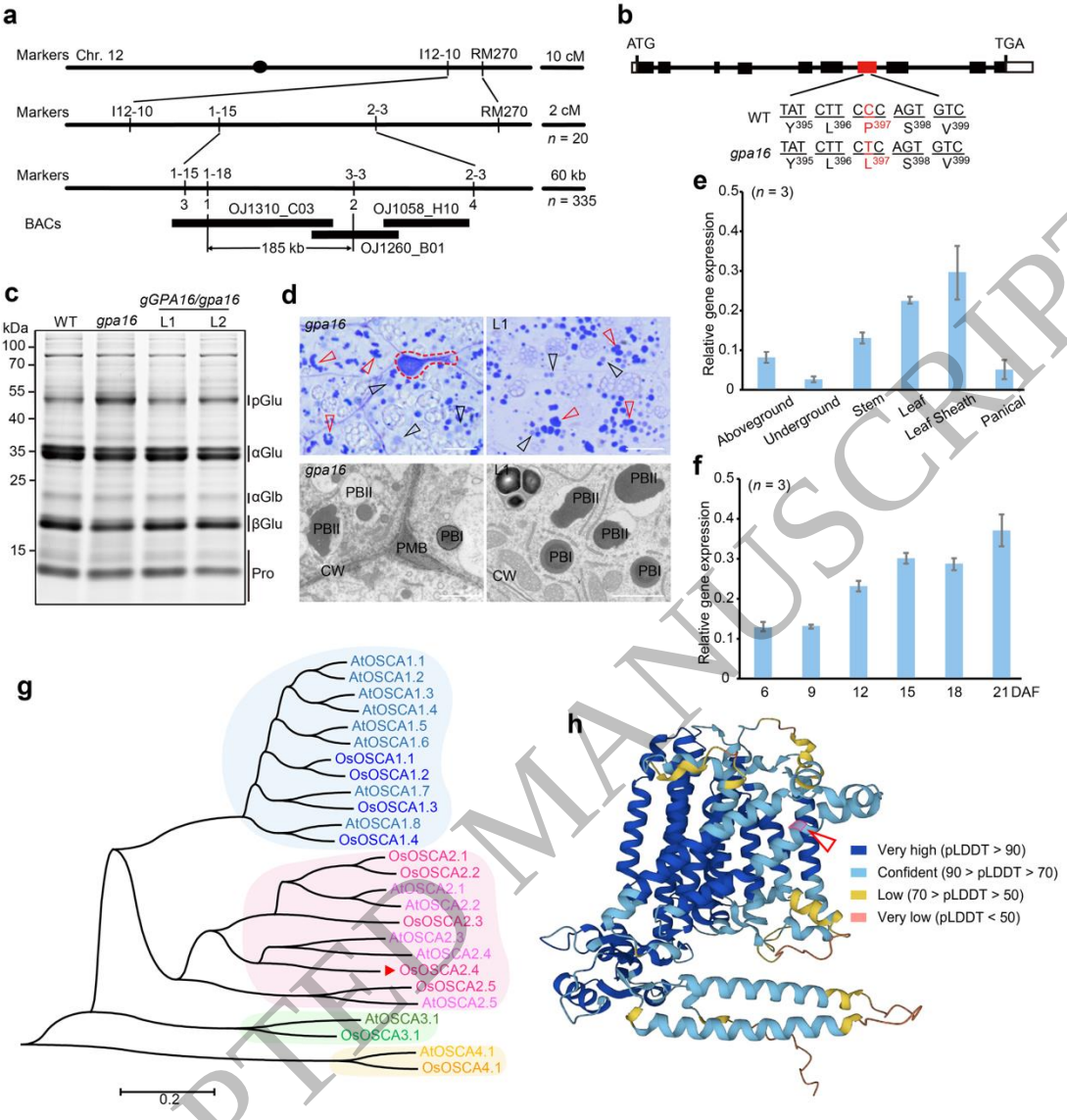

Figure 2. Map-based cloning of *GPA16* and characterization of the GPA16 protein.

(**a**) Fine mapping of the *GPA16* locus. The molecular markers, BACs, and the number of recombinants were shown. (**b**) Genomic structure and the mutation site of the *GPA16* gene. Solid boxes and lines denote exons and introns, respectively. ATG and TGA represent the start and stop codons, respectively. Red letters highlight the single-nucleotide substitution and the predicted amino acid residue variation between WT and *gpa16*. (**c**, **d**) An 8.6-kb genomic fragment of wild-type *GPA16* (*gGPA16*) rescued the proglutelin over-accumulation defect (**c**) and endomembrane trafficking defect (**d**) of proglutelins in *gpa16*. L1 and L2 indicate two independent T_2 transgenic lines. Light microscopy (upper panel) and transmission electron microscopy (lower panel) images of developing subaleurone cells of *gpa16* and representative transgenic line (L1). Red dotted line outlines the PMB structure,

ACCEPTED MANUSCRIPT

Downloaded from https://academic.oup.com/plcell/advance-article/doi/10.1093/plcell/koag193/8719692 by National Science & Technology Library user on 03 July 2026

black and red arrowheads in (**d**) indicate PBIs and PBIIs, respectively. pGlu, proglutelins; αGlu, glutelin acidic subunits; αGlb, α-globulin; βGlu, glutelin basic subunits; Pro, prolamins. Scale bars, 10 μm in (**d**, upper panel), 2 μm in (**d**, lower panel). (**e**, **f**) RT-qPCR analyses showing the *GPA16* expression pattern in various non-seed tissues (**e**) and developing endosperm tissues (**f**) examined. Aboveground and underground tissues were from 7-day-old seedlings. Stems, leaves, leaf sheaths, and panicles were from plants before heading. Values are means ± SD. DAF, days after flowering. (**g**) A neighbor-joining phylogenetic tree showing the predicted relationship of OSCAs in *Arabidopsis thaliana* (At) and rice (Os). (**h**) The predicted 3D structure of OsOSCA2.4 protein constructed using the AlphaFold (https://alphafold.ebi.ac.uk). The red arrowhead marks the proline residue substituted by leucine in *gpa16*.

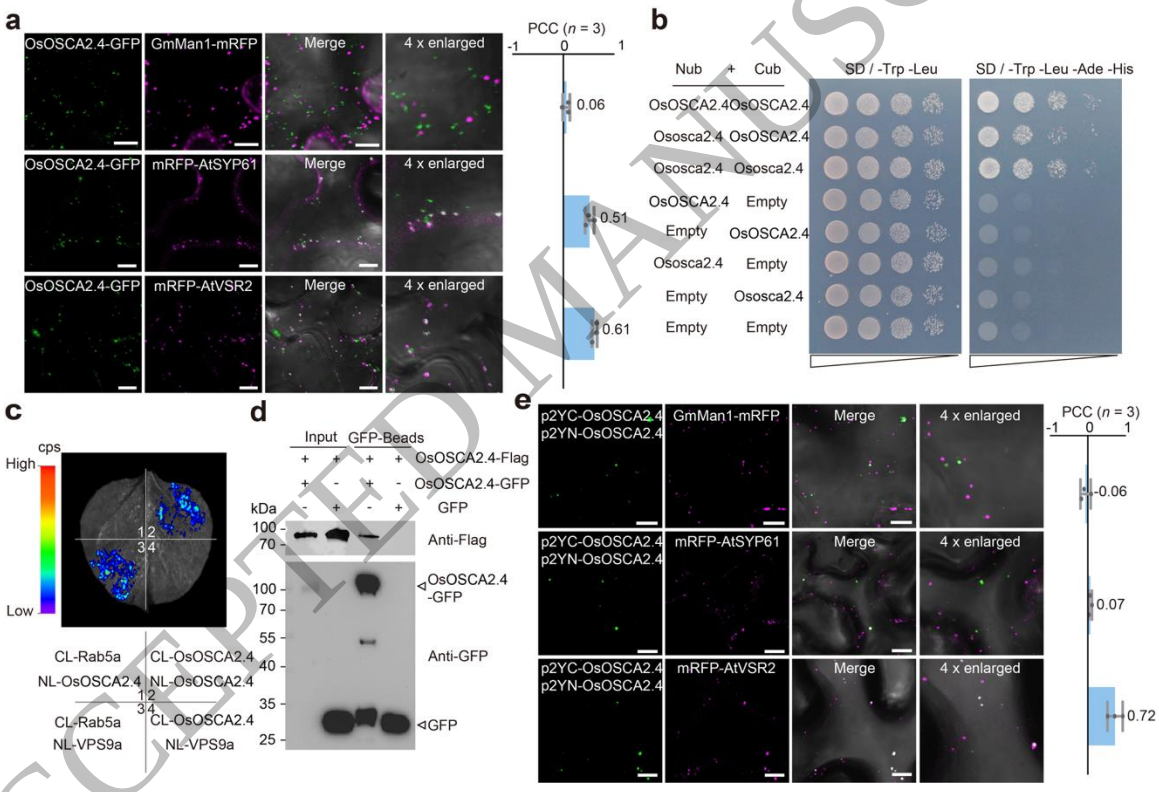

Figure 3. OsOSCA2.4 localizes to TGN and PVC in plants

(**a**) Confocal microscopy images showing the colocalization of OsOSCA2.4-GFP with mRFP-AtSYP61 (TGN marker) and mRFP-AtVSR2 (PVC marker) but not GmManI-mRFP (Golgi marker) in the leaf epidermal cells of *N. benthamiana*. The right panel shows PCCs for colocalization of OsOSCA2.4-GFP with each marker protein. Values are means ± SD. Scale bars, 10 μm. (**b**) Y2H assays showing the self-interaction of both OsOSCA2.4 and Ososca2.4. Nub, Nub fragment in the pXGY18 vector. Cub, Cub fragment in the pXGY17 vector. SD/-Trp-

ACCEPTED MANUSCRIPT

Downloaded from https://academic.oup.com/plcell/advance-article/doi/10.1093/plcell/koag193/8719692 by National Science & Technology Library user on 03 July 2026

Leu, Synthetic Dropout/-Trp-Leu; SD/-Trp-Leu-Ade-His, Synthetic Dropout/-Trp-Leu-Ade-His. (**c**) LCI assay showing that OsOSCA2.4 interacts with itself in *N. benthamiana*. The colored scale bar indicates the luminescence intensity in counts per second (cps). CL, C terminus of LUC; NL, N terminus of LUC. CL-Rab5a and NL-VPS9a serve as controls. (**d**) Co-IP assay showing that OsOSCA2.4-Flag could be co-immunoprecipitated in the total leaf protein extract of *N. benthamiana* with GFP-Beads. (**e**) BiFC assay verified the self-interaction of OsOSCA2.4 on PVC in *N. benthamiana*. PCCs between eYFP and each marker were shown on the right panel. Values were means ± SD. Scale bar, 10 μm.

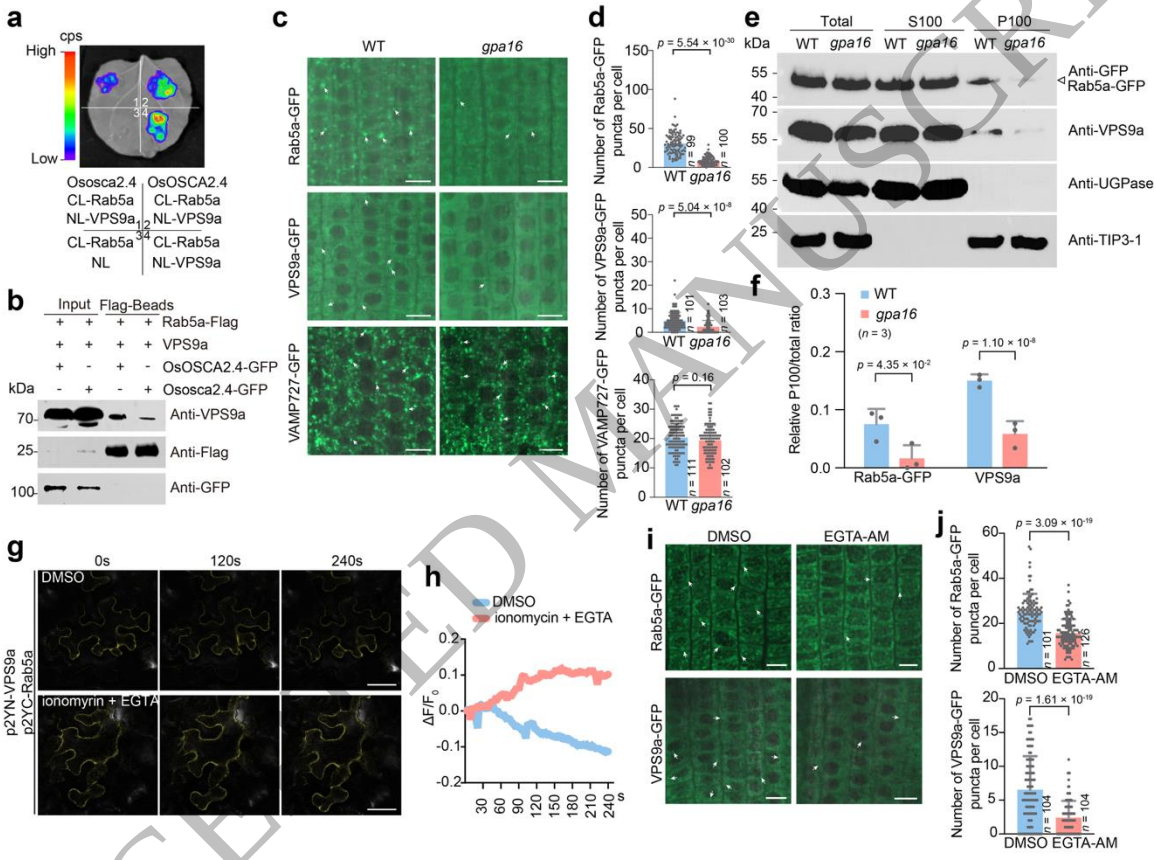

Figure 4. Ososca2.4 mutation and Ca^{2+} transients affect the membrane association of Rab5a and VPS9a.

(**a**) LCI assay verified the detrimental effect of Ososca2.4 on the interaction of Rab5a with VPS9a in *N. benthamiana*. Colored scale bar indicates the luminescence intensity in counts per second (cps). CL, C terminus of LUC; NL, N terminus of LUC. (**b**) Co-IP assay showing that *Ososca2.4* overexpression attenuates the interaction of Rab5a with VPS9a in *N. benthamiana*. (**c**) Confocal microscopy images showing that subcellular localization pattern of Rab5a-GFP, VPS9a-GFP, and VAMP727-GFP in root tip cells of WT and *gpa16*. White arrows indicate puncta. Scale bars, 10 μm. (**d**) Quantification of fluorescence puncta in (**c**).

ACCEPTED MANUSCRIPT

Downloaded from https://academic.oup.com/plcell/advance-article/doi/10.1093/plcell/koag193/8719692 by National Science & Technology Library user on 03 July 2026

Values are means ± SD. (**e**) Immunoblot analysis showing that the *Ososca2.4* substantially impairs the membrane association of Rab5a and VPS9a in developing endosperm. Anti-UGPase and anti-TIP3-1 antibodies were used as cytosol and membrane markers, respectively. (**f**) Quantification of Rab5a and VPS9a in P100 fractions in (**e**). Values are means ± SD. (**g**) Time-lapse BiFC imaging showing changes in Rab5a and VPS9a interaction (eYFP) after treatment with 10 μM ionomycin and 10 mM EGTA in *N. benthamiana*. DMSO was used as an experimental control. Scale bars, 50 μm. (**h**) Quantitative analyses of the interaction intensity changes in (**g**). eYFP fluorescence intensity was from images recorded in 3 s/frame for 240 s. $\Delta F/F_0$ depicted the relative interaction intensity changes, where F represented the real-time fluorescence intensity and F_0 represented the fluorescence intensity at time zero. $\Delta F = F-F_0$. (**i**) Confocal microscopy images showing that EGTA-AM treatment impaired the punctate localization of Rab5a-GFP and VPS9a-GFP in rice root tip cells. DMSO treatment was as an experimental control. White arrows indicate puncta. Scale bar, 10 μm. (**j**) Quantification of Rab5a-GFP and VPS9a-GFP fluorescence puncta in (**i**). Values are means ± SD. In (**d**), (**f**) and (**j**), statistical analyses were performed by two-tailed Student's *t* test.

ACCEPTED MANUSCRIPT

Downloaded from https://academic.oup.com/plcell/advance-article/doi/10.1093/plcell/koag193/8719692 by National Science & Technology Library user on 03 July 2026

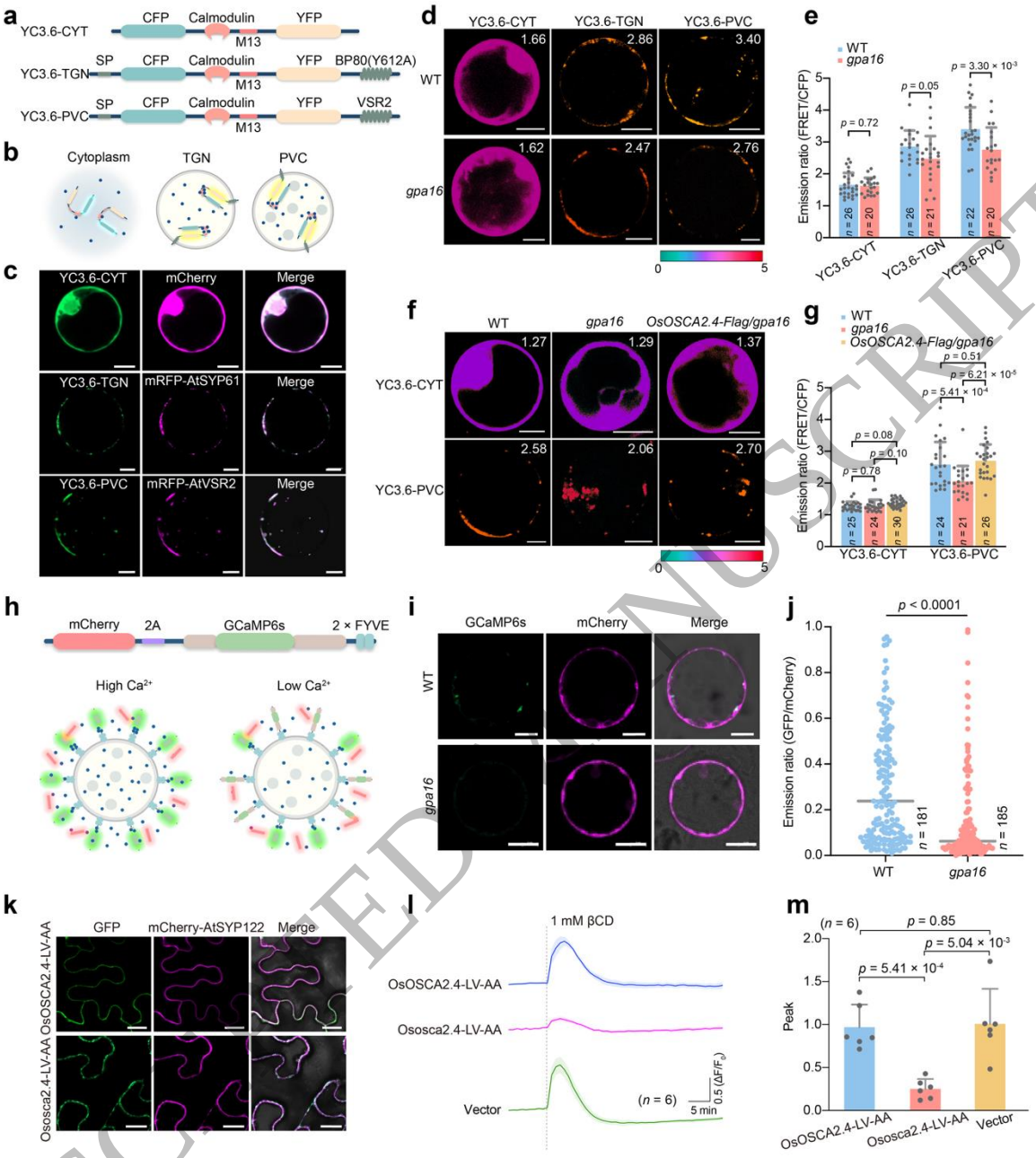

Figure 5. Ososca2.4 affects Ca^{2+} homeostasis within PVCs.

(**a**) Schematic representation of different YC3.6 biosensor constructs. (**b**) Working models of YC3.6 biosensor constructs in the cytosol, TGN, and PVC. CYT, cytosol. The blue dots indicate Ca^{2+}. (**c**) Colocalization of YC3.6 biosensors with markers characteristic for the cytosol, TGN, and PVC in rice protoplasts. Scale bars, 10 μm. (**d**) Representative pseudo-colored images of YC3.6-CYT, YC3.6-TGN, and YC3.6-PVC in protoplasts prepared from WT and *gpa16* seedlings. Data represent the mean FRET/CFP ratio. Colored scale bar indicates

ACCEPTED MANUSCRIPT

Downloaded from https://academic.oup.com/plcell/advance-article/doi/10.1093/plcell/koag193/8719692 by National Science & Technology Library user on 03 July 2026

the FRET/CFP ratio. Scale bars, 10 μm. (**e**) Ca^{2+} level represented by the emission ratio (FRET/CFP) of YC3.6 in the cytosol, PVC, and TGN of protoplasts prepared from WT and *gpa16* seedlings. Values are means ± SD. (**f**) Representative pseudo-colored images of YC3.6-CYT and YC3.6-PVC in protoplasts prepared from WT, *gpa16*, and *OsOSCA2.4-Flag* complemented seedlings. Data represent the mean FRET/CFP ratio. Colored bar indicates the FRET/CFP ratio. Scale bar, 10 μm. (**g**) Ca^{2+} level in cytosol and PVC of protoplasts prepared from WT, *gpa16*, and *OsOSCA2.4-Flag* complemented seedlings, quantified as the emission ratio (FRET/CFP) of YC3.6. Values are means ± SD. (**h**) Schematic representation of mCherry-2A-GCaMP6s-2×FYVE biosensor construct under high- and low- Ca^{2+} conditions. (**i**) The expression pattern of mCherry-2A-GCaMP6s-2×FYVE in the protoplasts isolated from WT and *gpa16* seedlings, respectively. Scale bars, 10 μm. (**j**) Ca^{2+} level quantified as the emission ratio (GFP/mCherry) of the mCherry-2A-GCaMP6s-2×FYVE biosensor in protoplasts prepared from WT and *gpa16* seedlings. Individual data points and means are shown. Gray lines represent the mean values. (**k**) Subcellular localization of OsOSCA2.4-LV-AA-GFP and Ososca2.4-LV-AA-GFP in leaf cells of *N. benthamiana*. mCherry-AtSYP122 was used as a PM marker. Scale bar, 20 μm. (**l**) Ca^{2+} imaging of OsOSCA2.4-LV-AA and Ososca2.4-LV-AA in leaf cells of *N. benthamiana* treated with 1 mM βCD. Empty vector was used as a control. F represented the real-time fluorescence intensity, and F_0 represented the fluorescence intensity at time zero. $\Delta F = F-F_0$. The dashed line marks the time of 1 mM βCD application. Values are means ± SEM. (**m**) Quantitative analysis of peak fluorescence levels. Peak = maximum response - baseline at zero added βCD. Values are means ± SD. In (**e**), (**g**), (**j**) and (**m**), statistical analyses were performed by two-tailed Student's *t* test.

ACCEPTED MANUSCRIPT

Downloaded from https://academic.oup.com/plcell/advance-article/doi/10.1093/plcell/koag193/8719692 by National Science & Technology Library user on 03 July 2026

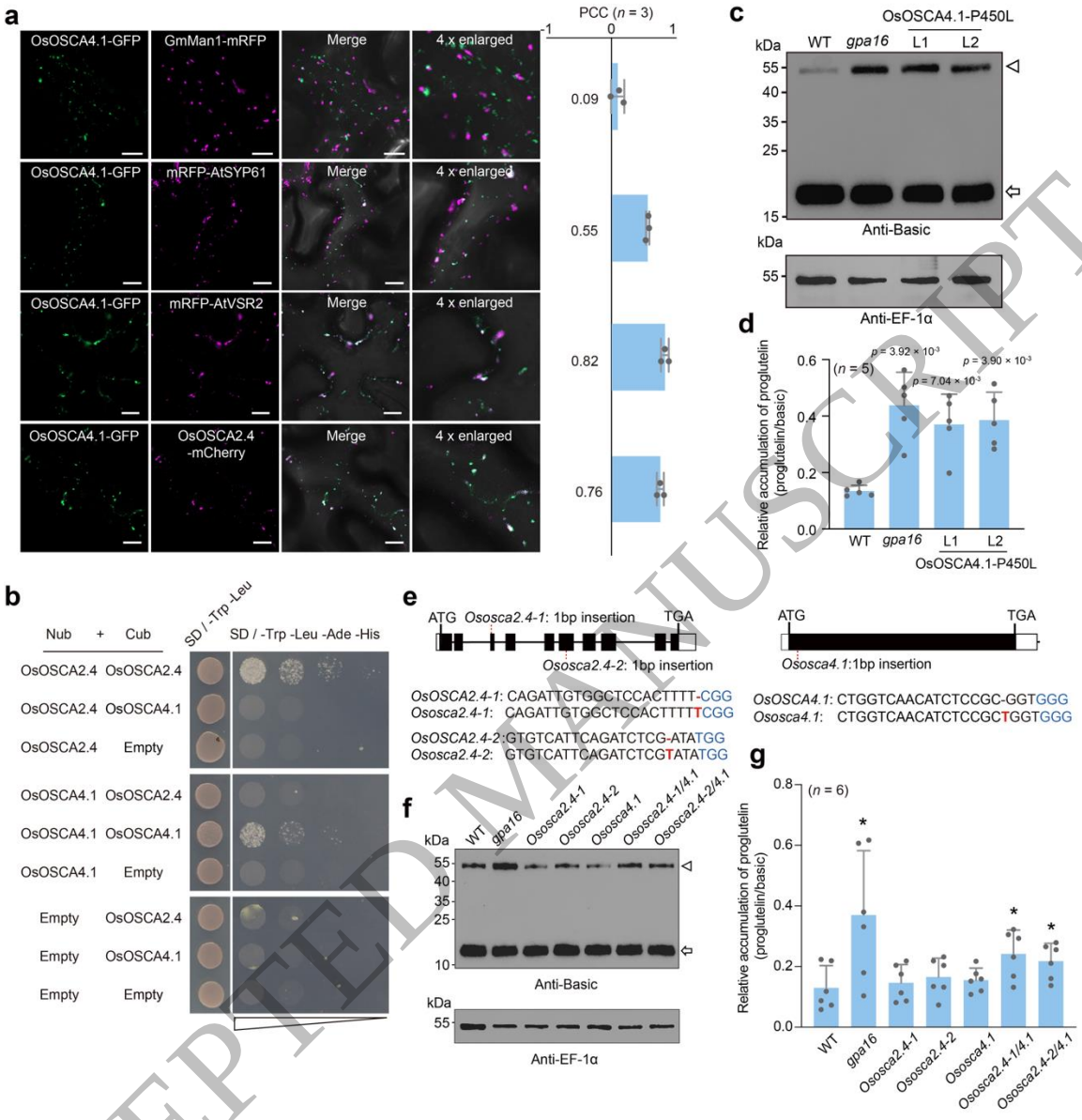

Figure 6. *OsOSCA2.4* acts redundantly with *OsOSCA4.1* to regulate proglutelins transport.

(**a**) Subcellular localization of OsOSCA4.1 in leaf cells of *N. benthamiana*. Scale bar, 10 μm. PCCs of OsOSCA4.1-GFP with each marker or OsOSCA2.4 were quantified by ImageJ. Values are means ± SD. Scale bars, 10 μm. (**b**) Y2H assay verifying the self-interaction of OsOSCA4.1. Nub, Nub fragment in the pXGY18 vector. Cub, Cub fragment in the pXGY17 vector. (**c**) Immunoblot analysis of OsOSCA4.1-P450L transgenic lines with antibodies against glutelin basic subunits. Anti-EF-1α was used as a loading control. Arrowhead indicates the proglutelins, while arrow indicates the glutelin basic subunits. (**d**) Relative band intensity of proglutelins/glutelin basic subunits in (**c**). L1 and L2 indicate two

ACCEPTED MANUSCRIPT

Downloaded from https://academic.oup.com/plcell/advance-article/doi/10.1093/plcell/koag193/8719692 by National Science & Technology Library user on 03 July 2026

independent transgenic lines. Values are means ± SD. (**e**) Gene structure and mutation sites of *OsOSCA2.4* and *OsOSCA4.1* genes. The solid boxes and lines denote exons and introns, respectively. ATG and TGA represent the start and stop codons, respectively. Red letters highlight the single base insertion and blue letters mark the PAM motifs. (**f**) Immunoblot analysis of mature seeds from single and double mutants of OSCAs using antibodies against glutelin basic subunits. Anti-EF-1α was used as a loading control. Arrowhead indicates the proglutelins, while arrow indicates the glutelin basic subunits. (**g**) Proglutelin accumulation levels (proglutelins/glutelin basic subunits) in single or double mutants relative to WT in (**f**). Values are means ± SD. In (**d**) and (**g**), statistical analyses were performed by two-tailed Student's *t* test. In (**g**), **P* = 0.039, 0.029, and 0.046, respectively.

ACCEPTED MANUSCRIPT

Downloaded from https://academic.oup.com/plcell/advance-article/doi/10.1093/plcell/koag193/8719692 by National Science & Technology Library user on 03 July 2026